J. Fluid Mech. (2008), *vol.* 608, *pp.* 243–274.
doi:10.1017/S002211200800205X Printed in the United Kingdom

On the wind-induced growth of slow water waves of finite steepness

WILLIAM L. PEIRSON[1] AND ANDREW W. GARCIA[2]

[1]Water Research Laboratory, School of Civil and Environmental Engineering, The University of New South Wales, King Street, Manly Vale, NSW 2093, Australia
W.Peirson@unsw.edu.au

[2]Coastal and Hydraulics Laboratory, US Army Engineer Research and Development Center, Vicksburg, Mississippi, USA

(Received 3 December 2007 and in revised form 15 April 2008)

Determining characteristic growth rates for water waves travelling more slowly than the wind has continued to be a key unresolved problem of air–sea interaction for over half a century. Analysis of previously reported and recently acquired laboratory wave data shows a systematic decline in normalized wave growth with increasing mean wave steepness that has not previously been identified. The normalized growth dynamic range is comparable with previously observed scatter amongst other laboratory data gathered in the slow wave range. Strong normalized growth rates are observed at low wave steepnesses, implying an efficient wave-coherent tangential stress contribution. Data obtained during this study show quantitative agreement with the predictions of others of the interactions between short wind waves and the longer lower-frequency waves. Measured normalized wave growth rates are consistent with numerically predicted growth due to wave drag augmented by significant wave-coherent tangential stress.

1. Introduction

An intriguing feature of all open water surfaces, subject to any but the lightest of winds, are the wind waves that form with lengths ranging from millimetres to hundreds of metres, given sufficient fetch and duration. Detailed investigations over at least 50 years have revealed the key role that waves play in the physical and constituent coupling between air and water (Jähne & Haußecker 1998; Janssen 2004). A particularly important class of waves within the field of air–sea interaction are what are termed *slow* waves.

Slow waves propagate at a speed c that is much lower than the prevailing wind velocity U_z specified at a height z above the mean surface (in terms of wind measured at the customary reference height of 10 m, the slow spectral component will consist of waves with $c/U_{10} < 0.2$). Present evidence is that it is the slow portion of the wave spectrum that supports a significant proportion of the wave-induced stress (Donelan 1990, p. 267; Makin & Kudryavtsev 2002; Janssen 2004, p. 214); is the primary contributor to enhanced air–water gas exchange and global geochemical cycling (Jähne & Haußecker 1998); and that plays a dominant role in many of the techniques used to sense sea surface and oceanic wind behaviour remotely (Robinson & Guymer 1996).

In spite of the widespread occurrence and the significant role of slow wind waves in the coupling of the atmosphere to open water, there is also a significant lack of fundamental understanding of key aspects of their behaviour. Perhaps the most important of these is the discrepancy between theoretical predictions of the wind-induced growth of slow non-breaking gravity waves forced by wind (Belcher & Hunt 1998) and available physical measurements. Van Duin (1996) concluded that 'present theories for wave generation by turbulent air flow do not take into account an (as yet unknown) essential wave growth mechanism, which enhances the growth rate significantly.'

Peirson, Garcia & Pells (2003) found strong wave attenuation when the wind is in the direction opposite to that of the waves. Also, a systematic relationship was observed between the mean wave steepness and energy fluxes from the wave field. This suggests that for the condition of wind aligned with slow waves and their consequent growth, further investigation is warranted into the significance of wave steepness in wind-forced wave behaviour.

The numerical study of Mastenbroek (1996) demonstrated a much stronger increase in the normalized growth rates of slow waves of finite steepness ($0.05 < ak < 0.3$) in response to mean steepness than occurred in response to wave age – the conventional normalizing parameter. Belcher (1999) found theoretically that by including a wave-coherent tangential stress contribution, the normalized growth of very low steepness waves decreases with increasing steepness. Donelan *et al.* (2006) found steepness to be an important factor in determining measured form drag levels above waves in the field.

This contribution examines the significance of mean steepness in determining wave growth rates, using previously and recently acquired experimental data. Mean wave steepness is shown to be an important factor determining the normalized growth rates of slow waves. In this paper, we review previous relevant investigations; describe new measurements obtained to resolve key outstanding issues; interpret these observations in the context of available theoretical models of wave growth; summarize the implications; and, identify key strategic future investigations.

2. Background

2.1. *A qualitative description of wind-forced slow wave behaviour*

As intrinsic wave frequency f increases within the slow wave domain, there are important transitions in wind-forced slow wave behaviour according to wavelength λ and mean steepness ak (a being wave amplitude and $k = 2\pi/\lambda$). Here, we provide a brief summary of the present understanding of the key transitions that occur within this complex domain (Kinsman 1984, pp. 46, 47).

The action of wind injects energy into the water surface via variations in pressure and surface shear. Viscous shear and propagating surface curvature in the presence of viscosity induces vorticity and a consequent energy dissipation (Longuet-Higgins 1992). Consequently, when wind forcing is weak ($<3\,\mathrm{m\,s^{-1}}$), viscous dissipation in the water is the dominant process and open water surfaces appear glassy and dominated by any pre-existing gravity wave fields.

When the winds exceed approximately $5\,\mathrm{m\,s^{-1}}$ (except at very short fetches $\sim < 3\,\mathrm{m}$), the surface becomes dominated by the microscale waves, accompanied by their attendant capillaries and lapsing in and out of a microscale breaking state (Katsaros & Atatürk 1992). It is unusual to observe fields of freely propagating capillary ripples, except at very short fetch, prior to gravity-wave formation. At approximately the

same wind speed threshold but at longer fetches, air entraining breaking commences (Holthuijsen & Herbers 1986, figure 7).

This paper discusses the response of slow waves to wind forcing. Whilst the role of surface tension in determining the dispersion of very short (slow) waves is widely appreciated (Phillips 1977, p. 37ff), surface tension and viscosity both indirectly play a key role in the appearance, behaviour and interactions of slow waves.

For very short waves (<50 mm approximately), surface tension effects are so strong and viscous dissipation is so high that they are rarely observed to break, either owing to direct wind-induced growth or long-wave modulation. Waves of slightly longer scale (approximately 50 mm to 500 mm) can break, but they can do so with negligible air entrainment – a process termed microscale breaking (Banner & Phillips 1974). Waves with lengths greater than approximately 0.5 m, break with air entrainment as popularly appreciated.

Another peculiar feature of waves with lengths of approximately 50–100 mm is that as they steepen, small *parasitic* capillary waves develop on their downwind faces. Parasitic capillary waves derive their energy from the underlying gravity wave. The details of parasitic wave formation have been described theoretically (Longuet-Higgins 1995). Blockage of capillary waves on short steep gravity waves (Shyu & Phillips 1990) contributes to parasitic capillary occurrence and the smooth appearance of the windward face and crests of steep short gravity waves.

In spectral systems, longer waves modulate shorter waves (Longuet-Higgins & Stewart 1960) and the modulation of short-wave surface curvature produces an uneven distribution of viscous dissipation along the long waves. Steeper short waves can break, thereby inducing two significant changes in wind–wave interaction: first, there is a significant increase in the momentum flux from wind to the waves (Banner 1990), and secondly, breaking induces a strong flux of momentum from the waves to the subsurface current (Duncan 1983; Rapp & Melville 1990; Banner & Peirson 2007).

2.2. *Wave growth theory*

Development of a wave field in response to wind forcing is expressed conventionally as an interaction of multiple processes, all of which have proved difficult to quantify. Using the notation of Komen *et al.* 1994 (§ I.2.5, p. 25ff), the local total energy density E of a spectrum surface wave propagating past a point can be evaluated as:

$$E = \rho_w g \langle \eta^2 \rangle = \rho_w g \iint \Phi(\omega, \theta)\, \mathrm{d}\omega\, \mathrm{d}\theta, \tag{1}$$

where ρ_w is the density of water, g is the acceleration due to gravity, Φ is the spectral energy density as a function of wave direction θ and wave angular frequency $\omega = 2\pi f$ and:

$$\Phi(\omega, \theta) = \tfrac{1}{2} a(\omega, \theta)^2. \tag{2}$$

The development of the wave field is usually described by the wave energy balance equation (Komen *et al.* 1994, pp. 33, 47):

$$\rho_w g \frac{\mathrm{d}\Phi(\omega, \theta)}{\mathrm{d}t} = S_{in}(\omega, \theta) + S_{nl}(\omega, \theta) + S_{diss}(\omega, \theta), \tag{3}$$

where S_{in} is energy input to the wave field by the wind, S_{nl} are energy transfers between wave frequencies due to nonlinear wave–wave interactions, and S_{diss} (a negative quantity) is the loss of energy from the wave field. The left-hand side of (3) uses the total derivative and therefore considers changes moving with the group

velocity of the spectral components. Direct measurement of any of the three terms on the right-hand side of (3) has proved extremely difficult. The subject of this investigation is the first term on the right-hand side of (3) for unidirectional wave fields co-aligned with the prevailing wind and, unless explicitly stated, directional effects will be neglected.

The action of wind induces both momentum and energy fluxes to open water surfaces. The total momentum flux or the wind stress τ is the sum of the tangential stress (τ_{tang}) and the form drag (τ_{form}):

$$\tau = \tau_{tang} + \tau_{form} = \langle \tau_{visc} / \sqrt{1 + (\partial\eta/\partial x)^2} \rangle + \langle p_s \partial\eta/\partial x \rangle, \tag{4}$$

where τ_{visc} is the local interfacial viscous shear stress and p_s is the pressure at the interface, $\partial\eta/\partial x$ is the local interface slope and the angle brackets denote temporal or spatial averaging.

There is wind-induced energy flux to both the waves and the surface currents. Assuming linear spectral decomposition of the wave field, the source term in (3) becomes:

$$S_{in}(\omega) = \langle \tau_{visc} u_s(\omega) \rangle + \langle p_s \partial\eta/\partial x(\omega) \rangle c(\omega), \tag{5}$$

where $u_s(\omega)$ is the surface velocity coherent with frequency component ω, $\partial\eta/\partial x(\omega) = -a(\omega)k(\omega)\sin(k(\omega)x - \omega t)$ and $c(\omega)$ is the wave speed. When normalized by wave speed, the first term of (5) is termed the wave-coherent tangential stress $\tau_{wc}(\omega)$ (see Longuet-Higgins 1969), and (5) becomes:

$$S_{in}(\omega) = (\tau_{wc}(\omega) + \tau_{form}(\omega))c(\omega) = \tau_{wave}(\omega)c(\omega). \tag{6}$$

Consequently, the momentum flux leading to wave growth $\tau_{wave}(\omega)$ has two components, the entire form drag and the wave coherent tangential stress.

Theoretical analysis of wave growth has primarily been led by the critical-layer theory developed by Miles (1957, 1962, 1993, 1996). Miles developed an analytical expression for the energy flux induced by airflow over a surface wave of small amplitude in the presence of a vertical logarithmic variation wind velocity above the surface. His expression takes the form:

$$\frac{S_{in}}{\omega E} = \beta \frac{\rho_a}{\rho_w} \left(\frac{u_*^a}{c} \right)^2, \tag{7}$$

where S_{in} is the energy input from the wind, β is a normalized growth coefficient, ρ_a is the density of air and the friction velocity is $u_*^a = \sqrt{\tau/\rho_a}$.

Miles' (1996) theory yields estimates of wind-wave growth as a function of wave age that are approximately 70% of the mean of assembled measurements (Plant 1982) by analysis of the air flow behaviour at the critical layer (where the wind speed is equal to the wave speed). This is a remarkable accomplishment given that the complexity of surface behaviour summarized in (4) to (6) is not considered. Van Gastel, Janssen & Komen (1985) improved the Miles (1962) analysis of the initial growth of gravity–capillary waves and obtained growth rates in reasonable agreement with the available measurements. Application of low-Reynolds-number turbulence models by Meirink & Makin (2000) yielded similar growth rates, and no further detailed consideration of the initial growth problem will be made here.

Further detailed analysis of the Miles theory, when applied to slow gravity waves, has shown that the critical height is too close to the wave surface for the Miles mechanism to be the primary contributor to finite-amplitude wave growth (Belcher & Hunt 1993; Miles 1996).

2.3. *Wave growth due to form drag*

Belcher & Hunt (1993) made theoretical estimates of other potentially significant interactions and found that the most significant contributor to low-steepness slow-wave growth was asymmetric surface pressure distribution which could be induced by non-separated airflow over the wave (so-called *non-separated sheltering*). This analysis reinvigorated interest in the work of Jeffreys (1925), who had previously developed an alternative theoretical expression for wave growth in the presence of separated airflow over the waveforms:

$$S_{in} = \tfrac{1}{2}\rho_{air} s_z (ak)^2 c^3 \left| \frac{U_z}{c} - 1 \right| \left(\frac{U_z}{c} - 1 \right), \tag{8}$$

where U_z and s_z are the wind speed and sheltering coefficient referenced at an elevation z above the mean surface.

However, Belcher & Hunt's theoretically predicted slow-wave growth rates were only approximately 50 % of the values measured experimentally. Belcher & Hunt (1993) also exposed a weakness of earlier numerical modelling of this problem: that the advection of turbulence over the undulating surface cannot be neglected, otherwise overestimates of wave growth rates are obtained. Subsequent detailed numerical model investigations (Mastenbroek 1996; Li, Xu & Taylor 2000) confirmed the findings of Belcher & Hunt and the significant difference between theoretical and measured growth rates of slow gravity waves remains (van Duin 1996).

2.4. *Wave-coherent tangential stress*

Longuet-Higgins (1969) developed a theory whereby energy could be imparted to surface waves by surface tangential stresses to form a wave-coherent tangential stress (equation (6)). He identified three methods by which surface tangential tangential stresses could be mediated and contribute to wave generation.

(i) *Direct wind-induced surface shear*

Investigations by Okuda, Kawai & Toba (1977) indicated the potential for direct wind-induced shear to be a significant wave-generation mechanism for short gravity waves. Their measurements using relatively large buoyant tracers yielded local tangential stress values at the wave crests to be up to 7 times larger than the total stress. However, measurements of wind shear within the viscous sublayer along the surfaces of microscale breaking waves obtained by Banner & Peirson (1998) yielded wave-coherent tangential stresses of approximately 10 % of the wind stress.

(ii) *Generation of surface shear by preferential viscous dissipation of capillary and gravity–capillary waves near the long-wave crests*

Theoretical studies by Longuet-Higgins (1992, for example) have shown that short waves are able to generate levels of viscous stress adjacent to their troughs that diffuse into the interior. This theoretical approach had been verified at larger scale by Longuet-Higgins (1960). Longuet-Higgins (1992) found that parasitic capillary waves of sufficient steepness have the potential to generate local viscous stresses that can be significantly larger that the wind stress.

(iii) *Generation of shear very close to the surface of longer waves but beneath the spilling regions of shorter breaking waves*

Modulation of the short-wave radiation stress has the potential to attenuate the long waves (Phillips 1963; Hasselmann 1971) but is negligible, provided that there is a sufficient separation in the frequency (speed) scales of the waves (Garrett & Smith 1976). Longuet-Higgins (1969) proposed that the higher speed of the long waves enables them to sweep beneath the short waves, the consequent orbital straining of

the short waves promoting injections of short-wave momentum which are strongly wave-coherent with the long waves. Garrett & Smith (1976) concluded that the long-wave modulation would promote a coherent modulation in the wave drag to the short waves that would be mediated locally to the long waves. The alternative models can be distinguished by whether the maximum short-wave energy is observed downwind or upwind (respectively) of the wave crests.

A complementary contribution has been made by Phillips & Banner (1974) who developed a model for short-wave breaking due to long waves. Their model predicts the reduction in short-wave energy that occurs owing to a combination of wind drift and the long-wave orbital motion. Their model was verified against their own data and that previously recorded by Mitsuyasu (1966). The Phillips–Banner model has been questioned by Wright (1976) who tested it against a broader range of wind speeds and monitored changes in short-wave energy using Doppler radar. Wright observed that the model was very effective at a single wind speed, but the predicted wave energy response due to long waves was inconsistent at higher and lower wind speeds. He postulated that this was because the Phillips–Banner contains no direct coupling to the wind.

The primary objection to a significant role for the wave-coherent tangential stress in S_{in} is that the wave orbital velocities require that the tangential stress be given a coefficient of order ak whereas there is no such requirement for the form drag (compare equations (13) and (14) in Peirson *et al.* 2003). As gravity wave steepnesses are of order 0.1, the magnitude of the wave coherent tangential stress estimated by Mastenbroek (1996) and measured by Banner & Peirson (1998) are in accord with this figure.

3. Measurements of slow wave growth

The conventional measurement benchmark for theoretical analysis was established by Plant (1982) from four data sets gathered in the field and the laboratory. The energy growth rates conformed to the quadratic dependence on inverse wave age (u_a^*/c) anticipated by Miles yet with normalized growth rates equivalent to $\beta = 32 \pm 16$, approximately a factor of 2 higher than that estimated by Miles (1957). Mitsuyasu & Honda (1982) concurrently published another set of data showing similar dependency on (u_a^*/c), but the growth rates measured by Mitsuyasu & Honda were approximately 50 % larger than those assembled by Plant.

3.1. *Measurement techniques*

There are four methods of measuring wave growth rates. These are reviewed briefly.

(i) *Electromagnetic Microwave Scattering*

There is a linear relationship between wave amplitude and Bragg scattered radar return from water surfaces (Larson & Wright 1975, p. 418) where the water wavelength matches the radar microwavelength. Consequently, radar can measure normalized net wave growth rates at very small wave steepnesses, with an accuracy that is difficult to achieve with other techniques. The primary application of this technique has been the initial growth of gravity–capillary waves, resolved by van Gastel *et al.* (1985) as discussed earlier.

(ii) *Pressure measurement in the air*

If the wave-coherent tangential stress is negligible and the surface static pressure can be extrapolated from pressure measurements above the interface, S_{in} can be obtained directly from surface pressure/slope correlation (Shemdin & Hsu 1967;

Donelan *et al.* 2006). The primary weakness of this technique is that the near-surface air flow is complex (clearly illustrated by Reul, Branger & Govanangeli 2007) and surface pressure extrapolations to the surfaces of steep, freely propagating waves are subject to unknown errors.

(iii) *Spatial changes of wave energy*

Conventional nonlinear wave interactions (Janssen 2004, chap. 4) are suppressed for monochromatic non-breaking wave fields subject to mild wind forcing (Bliven, Hwang & Long 1986; Peirson *et al.* 2003). In the absence of breaking, S_{in} can be obtained from (3) by measuring the net increase in wave energy along the fetch and correcting for viscous losses from the wave field (Wilson *et al.* 1973; Mitsuyasu & Honda 1982). If there are also losses due to turbulent effects (Teixeira & Belcher 2002; Peirson *et al.* 2003) such measurements will underestimate the magnitude of S_{in}. Such measurements cannot be undertaken in the presence of wave breaking because of a lack of precision in present estimates of energy loss from actively breaking waves (Rapp & Melville 1990; Banner & Peirson 2007).

(iv) *Tangential stress measurement*

Measurements of the viscous stress at the interface by Banner & Peirson (1998) yielded both the tangential stress and the wave coherent tangential stress measurements for microscale breaking waves. Deriving the form drag from (4), S_{in} can be obtained from (6). This technique has not been applied to longer gravity wave systems to date.

3.2. *Measurements of wave growth in relation to wave steepness available from the literature*

To investigate the potential role of wave steepness in determining slow wave growth, we undertook an extensive literature review to assemble measurements reported in the literature (table 1). Four of these studies were analysed by Plant (1982). The entire set is briefly described with our assessment of the availability of mean steepness data. Many investigators gathered the necessary information but, with the historical focus on the adequacy of Miles' theory (which does not anticipate a growth dependence on wave amplitude), wave steepness values have not been reported. Other investigators have reported wave steepness values at the point of initial wave generation, but did not report local representative values of ak, thereby excluding their data from further consideration. Where possible, errors have been computed and are presented for each data set.

Shemdin & Hsu (1967) and *Bole & Hsu (1969)*

These complementary studies were undertaken in the same facility. Their objective was to determine wave growth rates from near-surface pressure measurements (Shemdin & Hsu 1967) or spatial development of wave energy (Bole 1967, subsequently published as Bole & Hsu 1969). The wave growth rates implied by Shemdin & Hsu's pressure measurements were (on average) a factor of 3 less than the variation of spatial energy measurements of Bole & Hsu (1969). Resolution of the disparity between these studies has not been reported, to our knowledge.

Mean wave steepness values could not be derived from Shemdin & Hsu (1967), but by carefully reprocessing data from the original data of Bole (1967), we were able to obtain friction velocities and wave amplitudes. Bole's measurements were obtained prior to the wide availability of spectral filtering techniques and he obtained his estimates of wave amplitude by fitting an analytical streamfunction to his wave data using least-squares techniques. Such an approach has potential problems as it

Investigators	Technique	U_{cl} (m s^{-1})	U_{10} (m s^{-1})	$f = \omega/2\pi$ [Hz]	Number of data items	Remarks
Shemdin & Hsu (1967)	Static air pressure	2.9–6.6		0.4	6	Wave follower. Reprocessing data was not possible during this study.
Bole (1967)/Bole & Hsu (1969)*	Spatial chnage of wave energy	3.7–12.5	4.8–17.7	0.9–1.4	28	Data were reprocessed to obtain mean steepness value, friction velocities and normalized growth rates for non-breaking waves.
Wilson *et al.* (1973)*	Spatial change of wave energy	1.1–1.9	1.7–2.8	2.01–6.04	10	Data was reprocessed to obtain mean steepness values although these data lie in the capillary–gravity range.
Snyder *et al.* (1981)	Static air pressure				87	Field study. The sophisticated processing undertaken could not be repeated during this present study. See also Hasselmann and Bösenberg (1991)
Larson & Wright (1977)	Radar				26	Mean steepness values could not be obtained from this data.
Wu, Hsu & Street (1979)	Static air pressure	7.1–8.8		Wind wave spectra	26	A detailed re-examination of the data obtained during this study was not able to obtain reliable mean steepness values or normalized wave growth rates.
Mitsuyasu & Honda (1982), figure 9*	Spatial change of wave energy	10	15.1	1.43	5	Limited surface energy measurements were reviewed in detail during current investigation.The larger body of data is shown in their figure 11, but it could not be reprocessed.
Bliven *et al.* (1986)*	Spatial change of wave energy	Not reported		2.0	8	Wind forcing quantified in terms of u_*^a, no aerodynamic roughness lengths were reported. Data herein does not include four sets of wave growth data which exhibited energy loss due to breaking and were unsuitable for reprocessing.
Banner (1990)*	Static air pressure	5.5	8.3–10.0	2.85, 3.35	4	Pressure measurements obtained at fixed elevations.
Mastenbroek *et al.* (1996)*	Static air pressure	5.4, 6.3	6.6, 7.7	1.4	2	Pressure measurements obtained at fixed elevations.
Banner & Peirson (1998)*	Tangential stress measurement	4.8–8.1	6–11	3.0–5.0	6	Wind input to wave field obtained from computed from drag added to wave-coherent tangential stress.
Donelan (1999)	Static air pressure	Not reported		$f_p = 2.01$ Hz	Many	Wave follower measurements of growth and attenuation. JONSWAP spectra. Data could not be reprocessed for this study.
Donelan *et al.* (2006)	Static air pressure		7.1–12.0	0.54–1.14	Many	Field study with measurements in fixed and following mode.
Present investigation*	Spatial change of wave energy	5.0, 6.8	7.0, 9.3	1.18, 1.67	24	

*Studies from which wave growth data could be related to mean wave steepness.

TABLE 1. Summary of reported measurements of wave growth.

is unable to distinguish between long-wave and shorter-wind wave fields which are usually developing simultaneously with the fetch.

Wilson et al. (1973)

Wilson *et al.* (1973) completed a delicate set of spatial development of wave energy measurements under very light wind conditions. To relate their net (observed + corrections for viscous decay) amplitude growth rates as a function of wave frequency and wind forcing to mean wave steepness, the data used in this present study were obtained by reprocessing the data presented in their figures 5 to 9. Wilson *et al.* (1973) showed that attenuation rates approached viscous estimates as the wind forcing was reduced. Their data spanned the capillary–gravity into the gravity wave range of frequencies.

Larson & Wright (1975)

Larson & Wright (1975) employed radar to measure the initial growth rates of waves with wavelengths ranging from 7.2 mm to 70 mm in response to impulsively applied wind forcing. There is some uncertainty regarding surface forcing during these experiments (see Donelan & Pierson 1987, p. 4975) and no direct determination of the mean wave steepnesses is possible.

Wu, Hsu & Street (1979)

Wu *et al.* (1979) used similar techniques to those used by Shemdin & Hsu (1967), but applied them to rapidly growing wind-generated waves. These laboratory experiments were designed to examine the development of wind-wave spectra.

Wu *et al.* (1979) is a summary of the results presented in Wu *et al.* (1977). The original data contained in Wu *et al.* (1977) were carefully re-examined by Peirson & Belcher (2005) but they were unable to obtain mean steepness values nor reproduce their normalized wind input values during reanalysis.

Snyder et al. (1981)

Snyder *et al.* (1981) describe data gathered under field conditions using an array of fixed and wave-following air-pressure sensors in the Bight of Abaco. They reported that waves of higher frequency than could be monitored with their instrumentation were supporting a significant proportion of the total stress. The signal processing undertaken was complex and could not be reviewed in detail during this study. A similar investigation by Hasselmann & Bösenberg (1991) found similar wave growth rates to Snyder *et al.* but the results of this later study also could not be reprocessed.

Mitsuyasu & Honda (1982)

Using spectral filtering of surface elevation records, Mitsuyasu & Honda (1982) investigated the growth of monochromatic, mechanically generated waves by wind for water surfaces in the presence and absence of a surfactant. Unfortunately, it was not possible to reprocess the Mitsuyasu & Honda data to obtain mean steepness values at mid-fetch for only the five measurements obtained from their figure 9.

Bliven et al. (1986)

Bliven *et al.* (1986) showed that wind forcing suppresses the formation of Benjamin & Feir (1967) sidebands on mechanically generated monochromatic waves monitored using surface elevation probes. Eight measurement results for non-breaking wind-forced monochromatic mechanically generated waves could be extracted from their table 3 and appropriate corrections for viscous attenuation were applied.

Banner (1990)

Banner (1990) investigated the changes in total drag and form drag over short mechanically generated waves at the transition from incipient to microscale breaking. The form drag was obtained from air pressure/wave slope correlations. It was observed that the form drag and total drag both approximately doubled with the transition to the breaking condition. However, the ratio of form drag to total drag remained approximately the same for steep non-breaking and continuous breaking wave conditions.

Mastenbroek et al. (1996)

Air flow measurements were taken above monochromatic mechanically generated waves in the large wind-wave tank in Marseille. The specific objectives of this investigation were to verify theories regarding rapid distortion of turbulence in the air flow above the waves. However, from the air pressure/slope measurements, two estimates of form drag can be obtained by extrapolating their pressure data to the mean water level and thereby yielding estimates of wind-induced wave growth rates.

Banner & Peirson (1998)

Banner & Peirson (1998) quantified the magnitude of the tangential stress and the wave coherent tangential stress at the surfaces of wind-forced microscale breaking waves using particle-image velocimetry at very high resolution, as discussed earlier.

Donelan (1999)

Donelan (1999) used a surface-following pressure probe tracing the wind-forced surface of waves generated with a JONSWAP spectral distribution by a paddle in a laboratory tank. Experiments were undertaken with the wind and the waves aligned in the same direction and with the wind opposed to the direction of wave propagation. The Jeffreys (1925) growth sheltering coefficient of $s_{\lambda/2}$ was found to be 0.28. Very limited supporting data was available within this paper and the growth data could not be reprocessed in terms of wave steepness.

Donelan et al. (2006)

Donelan *et al.* (2006) used a wave follower to measure near-surface static pressure in the field. The measurements were undertaken above waves in transitional water under moderate wind forcing ($U_{10} = 7$ to $10\,\mathrm{m\,s^{-1}}$) with slow-wave conditions at the spectral peak. They reported that incorporating a parameterization of air-flow separation was important to collapsing their data set. Their expression is:

$$\frac{S_{in}}{\omega E} = \frac{\rho_a}{\rho_w} G a k \left(\frac{U_{\lambda/2}}{c} - 1 \right)^2, \tag{9}$$

where the coefficient G takes different values according to whether air-flow separation has been initiated:

$$G = \begin{cases} 4.91; & ak(U_{\lambda/2}/c - 1)^2 < 1, \\ 0.93; & ak(U_{\lambda/2}/c - 1)^2 \geqslant 1, \end{cases} \tag{10}$$

although this threshold predicts air-flow separation at steepnesses that are much lower that observed during laboratory experiments (Banner 1990; Reul *et al.* 2007).

Donelan *et al.* (2006) also proposed a possible revision of the value of 0.28 found by Donelan (1999) down to 0.17 based on a re-examination of the spectral definitions previously used to process the laboratory data.

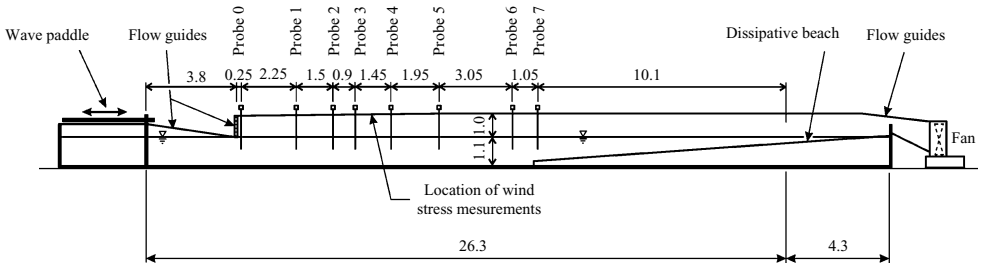

FIGURE 1. Layout of the facility; dimension in metres.

4. Measurements undertaken during this investigation

Phillips (1985, p. 510) observed that the growth coefficients obtained by Mitsuyasu & Honda (1982) seem implausibly high. Yet, to date, no quantitative reconciliation of the Mitsuyasu & Honda results to other measurements (e.g. Plant 1982) has been undertaken, even though the normalized growth rates obtained by Mitsuyasu & Honda are a factor of 1.5 higher, on average. Definitively resolving this issue required that new measurements be taken in a similar manner. Measuring the spatial rate of change of wave energy was used to determine wave growth rates during this present study.

From this point, we must distinguish carefully between the characteristic properties of mechanically generated low-frequency (so-called *long*) waves and the accompanying short wind-generated waves. We do this by using lower case variables to denote short-wave characteristics (a amplitude, f intrinsic frequency, c wave speed and k wavenumber) and upper case for those of the long waves (A amplitude, F intrinsic frequency, C wave speed and K wavenumber).

4.1. *Wind-wave facility*

A test facility of appropriate size and dimension was selected to carefully re-examine the Bole & Hsu (1969) and Mitsuyasu & Honda (1982) growth rates for monochromatic mechanically generated (so-called *long*) waves in the absence of surfactants. This present study was undertaken in the 0.9 m wide wave tank at the Water Research Laboratory (length 30.6 m, water depth 1.0 m) in the configuration shown in figure 1. This facility was used previously for the wind-induced wave attenuation study of Peirson *et al.* (2003) in a slightly different configuration.

Waves are generated by a controlled random generator at one end of the tank. During the present investigation, only monochromatic waves were investigated. At the far end of the tank from the generator, a dissipating beach was installed. It had been previously shown that the waves reflected from the beach had amplitudes less than 2 % of the incident mechanically generated waves (Peirson *et al.* 2003).

On each day of testing, prior to any measurements being obtained in the facility, a steady wind of $6.8\,\mathrm{m\,s^{-1}}$ was applied to the tank for a duration of one hour. This had the effect of ensuring that any floating material was either subducted and mixed down into the water column by the wind-generated microscale breaking waves or deposited on the beach at the downwind end of the tank. Visual inspection confirmed that this process was effective in removing films from the tank surface.

Nominal windspeed U ($\mathrm{m\,s^{-1}}$)	Long-wave frequency F (Hz)	Long-wave mean steepness AK	Air friction velocity $u_a^* \pm 5\,\%$ ($\mathrm{m\,s^{-1}}$)	Aerodynamic roughness $z_0 \pm 25\,\%$ (mm)	U_{10} ($\mathrm{m\,s^{-1}}$)
5.4	1.67	0	0.309	0.340	7.96
5.4	1.67	0.055	0.267	0.167	7.34
5.4	1.67	0.112	0.277	0.179	7.56
5.4	1.67	0.178	0.293	0.294	7.65
5.4	1.17	0	0.309	0.340	7.96
5.4	1.17	0.020	0.275	0.228	7.35
5.4	1.17	0.045	0.256	0.154	7.11
5.4	1.17	0.068	0.248	0.114	7.06
6.8	1.67	0	0.365	0.279	8.49
6.8	1.67	0.071	0.347*	0.170	8.46
6.8	1.67	0.141	0.333*	0.122	8.35
6.8	1.67	0.208	0.327*	0.109	8.28
6.8	1.17	0	0.365	0.279	8.49
6.8	1.17	0.018	0.352	0.278	9.23
6.8	1.17	0.044	0.335	0.164	9.22
6.8	1.17	0.070	0.332	0.146	9.23

*See note in text.

TABLE 2. Summary of measured wind forcing and long wave characteristics obtained during the present experimental study.

4.2. *Wind stress measurements*

Air flow in the facility was from left to right in figure 1. Flow guides were installed at the inlet to ensure that the incoming air flow transitioned smoothly to the water surface at the commencement of the test section.

The wind stress was measured mid-way along the test section (figure 1). However, Peirson *et al.* (2004, referred to in Makin *et al.* 2007) found a significant response in the measured wind stress to the steepness of long waves. To minimize uncertainty in the wind stress, the indirect logarithmic profile method was avoided and the stress was determined directly via the eddy-correlation method using constant-temperature wire anemometers in a cross-configuration.

The vertical dimension of a laboratory tank constant stress layer is determined by the total air cavity depth, which was increased to the maximum feasible in this facility (1.0 m). The roof was profiled to achieve a zero pressure gradient along the test section and these modifications yielded a constant stress layer to a height of 45 mm above the still water surface for centreline wind speeds up to $6.8\,\mathrm{m\,s^{-1}}$. The expensive high-resolution wire anemometers are destroyed by contact with water, thereby applying a practical limit to the wave heights (and therefore wave steepnesses) that could be investigated. For each wind speed and wave period case, four measurements of the turbulent stress across each steepness range were obtained and intermediate values of stress obtained by linear interpolation. The primary measurements obtained are summarized in table 2.

A minor problem with the wind forcing measurements for $U = 5.4\,\mathrm{m\,s^{-1}}$, $F = 1.67\,\mathrm{Hz}$ is that the friction velocities measured in the absence of the long waves were found to be 9 % less than reference measurements obtained during the early stages of the study. Unfortunately, this problem did not become apparent until well after the experiments were completed (and the wind tunnel dismantled). As the

steepness-dependent measurements for this condition were all systematically 10 % lower than those obtained at the same wind speed and $F = 1.17$ Hz, all friction velocities in the presence of long waves at $U = 5.4\,\mathrm{m\,s^{-1}}$, $F = 1.67$ Hz have been increased by a constant factor of 9 % to obtain the most accurate estimates of friction velocity in this case.

4.3. *Wave measurements*

Water surface elevation was monitored using capacitance wave gauges fitted with fine (~200 μm diameter) wire filaments with a water level range of approximately 200 mm. These were regularly calibrated and, over the period of testing, showed a gain repeatability better than 2 %. Probes were located at distances of 2.25, 3.75, 4.65, 6.10, 8.05, 11.10 and 12.150 m from the first probe within the roofed section which was located 0.25 m downwind of the entrance to the wind-wave tunnel (see figure 1). Outputs were digitised at 333 Hz per probe by a computer with an analogue to digital converter and the results stored for subsequent processing. Visual inspection confirmed that no long-wave breaking occurred within the test section.

4.4. *Data processing*

Peirson *et al.* (2003) had previously used wave energy measurement and filtering techniques very similar to those used by Mitsuyasu & Honda (1982). During the present study, the sample size was increased to 8192 data points which were processed from each record using fast Fourier transforms (FFTs) to determine the local wave energy. The higher digitization rate and larger sample size used in the present study enabled more accurate characterization of the long-wave spectral peak (figure 2). The entire long-wave energy is captured within the spectral band of the long-wave frequency and the immediately adjacent frequency bands. These values were added to obtain the local long-wave energy. Note that there is negligible (<1 %) leakage during spectral analysis to other frequency bands.

The sensitivity of these measurements is illustrated in figure 2(*a*). Although the mean steepness of the long waves is only 0.018, the spectral peak associated with the long waves is clearly defined in the spectrum. Figure 2 also exhibits the behaviour associated with increasing the steepness of the long waves as observed by many previous investigators: wind-wave energy is suppressed; and, long-wave nonlinearity increases and side bands develop with fetch (figure 2*b*). These features were neglected when computing the long-wave energy, resulting in a potential underestimation of wave energy by up to 5 % at the longest fetches and for the steepest conditions investigated. However, any reduction in measured growth rate will remain less than a few per cent.

Wave growth is a very delicate process in comparison with attenuation by opposing wind (Peirson *et al.* 2003, figure 6). Nonetheless, consistent growth rates were obtained amongst the repeat experiments undertaken within the facility and, notably, systematic behaviour was observed as a function of wave steepness. This is illustrated in figure 3, where the measured energy variation with fetch is shown across a range of long-wave steepness values. For the lowest steepness case, four independent measurements are shown with the computed mean to illustrate their repeatability.

To determine S_{in}, a spatial dimensional growth rate Δ was determined from the measured data by a least-squares fit of the equation:

$$E = E_0 \mathrm{e}^{\Delta x}, \tag{11}$$

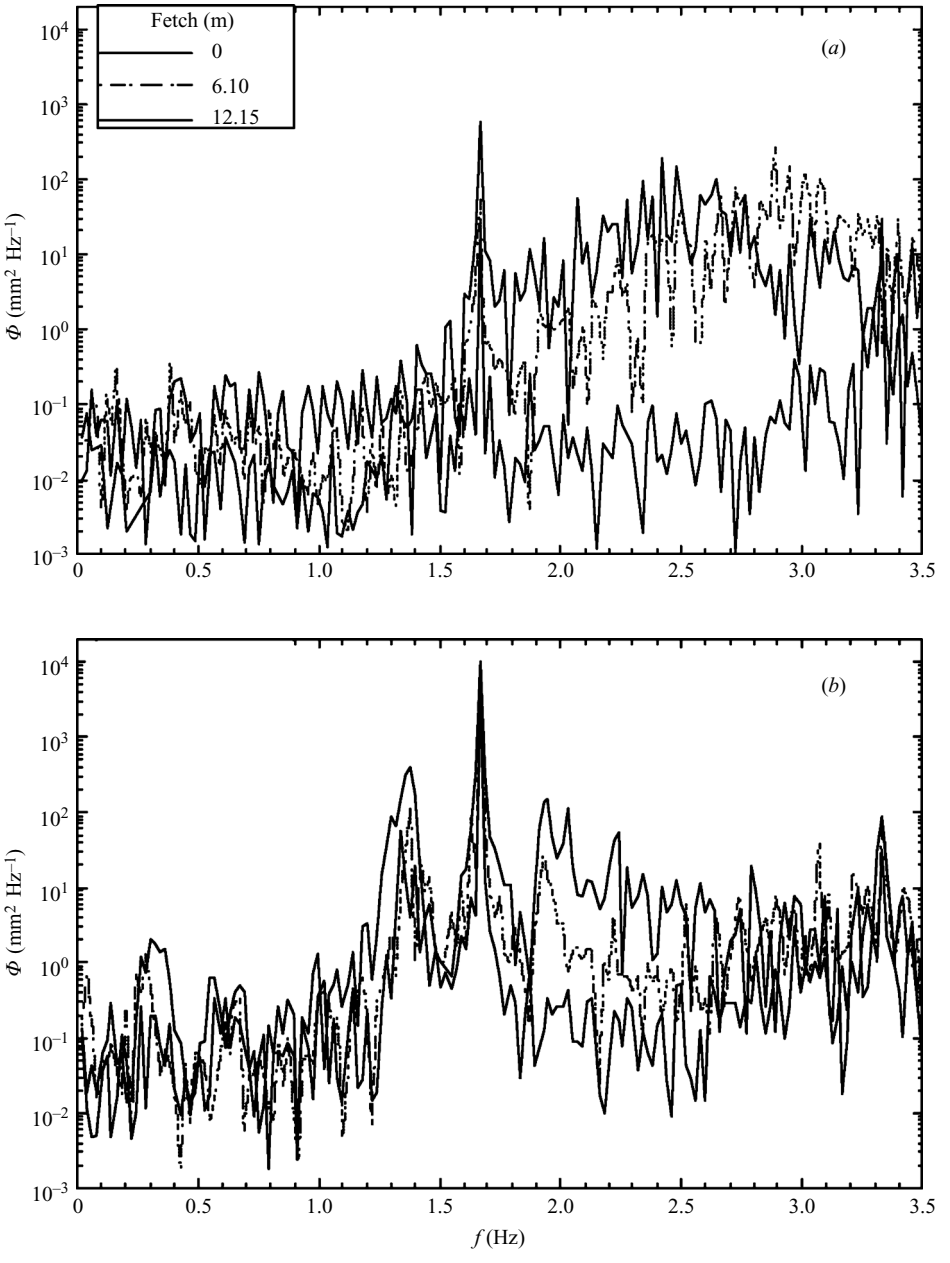

FIGURE 2. Spectra obtained at three fetches during the investigation. Line styles indicate fetch. $F = 1.67\,\mathrm{Hz}$, $U = 6.8\,\mathrm{m\,s^{-1}}$ (*a*) $AK = 0.018$. Note the clearly defined spectral peak and wind wave spectra that develop with fetch. (*b*) $AK = 0.208$. Note the clearly defined spectral peak, side bands and harmonic as well as the greatly reduced wind-wave spectral energy relative to that shown in (*a*).

where E is the extracted long-wave energy and x is the distance along the fetch. The wind input to the wave field was determined from:

$$S_{in} = \tau_{wave} C = (\Delta + \Delta_{visc}) C_g \langle E \rangle, \tag{12}$$

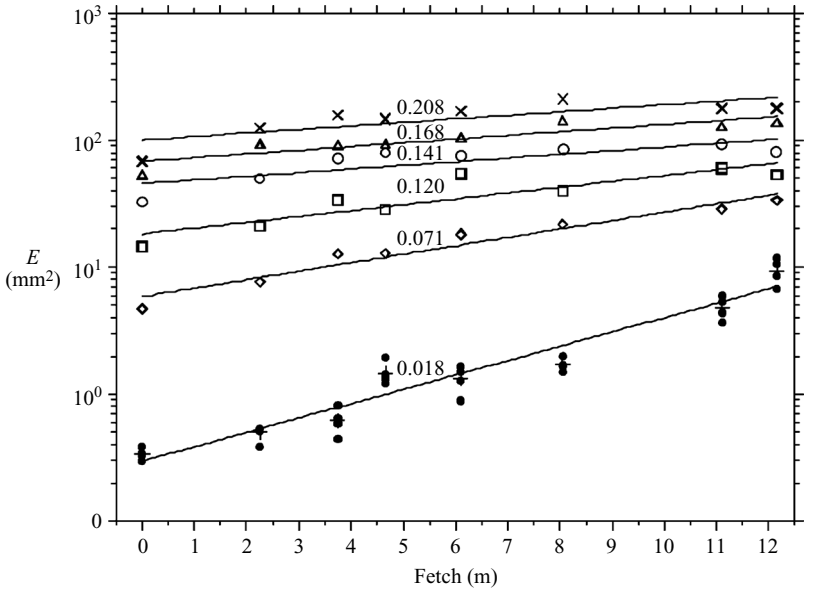

FIGURE 3. Development of long-wave energy with fetch for the case $F = 1.67$ Hz, $U = 6.8\,\mathrm{m\,s^{-1}}$ of the present study. Large symbols show mean energy values obtained from measurement ensembles. For the lowest mean long-wave steepness case, variation within the repeat measurements are shown as solid circles. Net wave growth was determined numerically from the best-fit lines shown.

where $\langle E \rangle$ is the long-wave energy at the mid-point of the fetch, C_g is the long-wave group velocity and Δ_{visc} is the estimated attenuation rate due to viscosity at the surface and the walls of the tank (the expression developed by Van Dorn 1966 was previously verified in the absence of wind by Wilson *et al.* 1973 and Mitsuyasu & Honda 1982).

5. Data analysis

5.1. *Wave drag and normalized growth*

Figure 4 is a collation of normalized growth rates of the data assembled by Plant (1982) with the additional growth data obtained from the literature and the growth measurements of this present investigation. Assembling the additional data in this fashion does not yield a satisfactory collapse although some data sets are clearly very noisy. The following observations can be made.

1. In spite of the systematic behaviour observed in the raw measurements obtained during this investigation, this normalization does not provide a systematic means of collapsing the data.

2. The five points that could be reprocessed from Mitsuyasu & Honda (1982) yield values in the vicinity of the upper Plant bound, but at the lower bound of the Mitsuyasu & Honda data envelope.

3. Regression re-analysis yielded 90 % confidence limits from measurements of the development of wave energy along the fetch (cf. Peirson *et al.* 2003). However, taking these into account still does not yield a deterministic mean value. Significant scatter remains about the mean value obtained by Plant that cannot be accounted for in terms of experimental error.

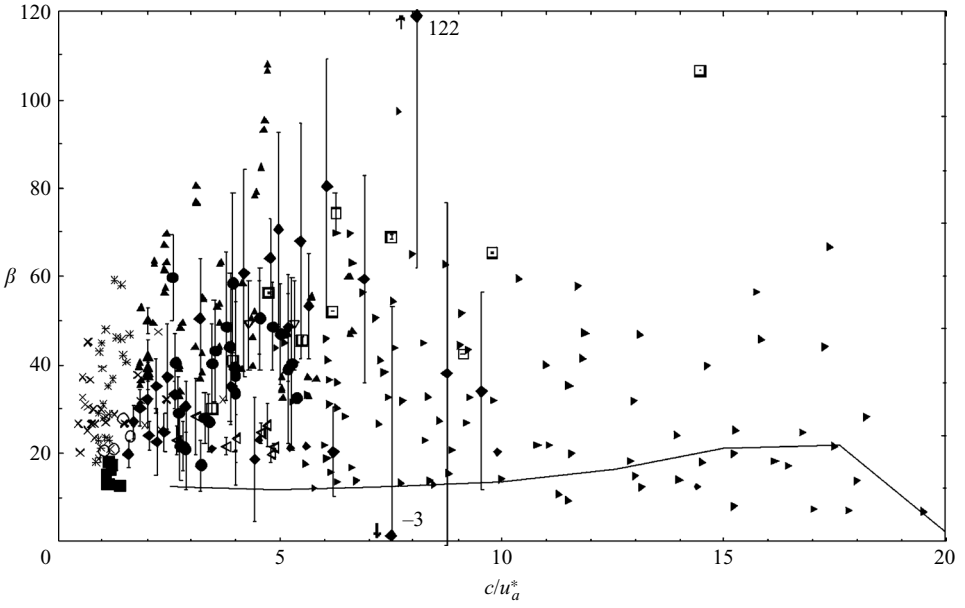

FIGURE 4. Normalized wave growth data assembled by Plant (1982) supplemented with data extracted from other investigations. Error bars indicating 90 % confidence as shown where these could be computed. Grey asterixes, Larson & Wright, 1974; grey x, data from Wu, Hsu & Street 1977; grey diamonds, Shemdin & Hsu 1967; grey triangles to right, Snyder *et al.* 1981; black diamonds, Bole 1967; black open squares, Wilson *et al.* 1973; black open circles, Banner 1990; black open triangles to left, Bliven *et al.* 1986; upright triangles, Mitsuyasu & Honda 1982; downward pointing triangles, Mastenbroek *et al.* 1996; solid squares, Banner & Peirson 1998; solid circles, present study. The second-order turbulence closure results computed by Mastenbroek (1996) are shown as a solid line.

4. The data of Wilson *et al.* (1973) exhibit an apparent systematic increase in normalized growth rate with increasing wave age.

5. Additional assembled data reinforces the disparity between the measured data and theoretical estimates of wave growth as represented by the results of Mastenbroek (1996).

Combining equations (6) and (7) with first-order Stokes approximations yields (Townsend 1972):

$$\frac{S_{in}}{C\tau} = \frac{\tau_{wave}}{\tau} = \frac{1}{2}\beta(AK)^2. \tag{13}$$

With the Plant mean value of $\beta = 32$, equation (13) yields the light solid curve shown in figure 5 in comparison with those data for which steepness could be computed. When presented in this manner, a number of features in the data become apparent.

1. The data measured in this study collapse systematically around a common curve from zero steepness up to the maximum mean steepness value that could be measured without wave breaking commencing within the test section. Notably, even for the very low steepnesses shown in the inset panel, there is good data collapse.

2. Therefore, analysis of slow-wave data in terms of steepness is useful in ordering the data that is not possible in terms of wave age. As shown by more recent numerical modelling, normalized growth of slow waves is weakly related to wave age, but strongly influenced by wave steepness (compare the results of Mastenbroek 1996 shown in figures 4 and 5).

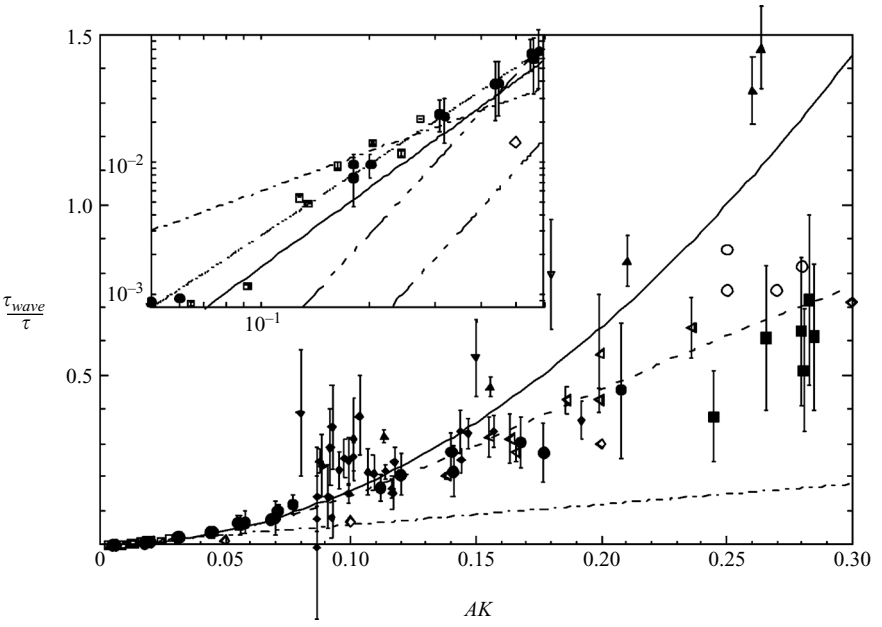

FIGURE 5. Computed wave drag plotted as a proportion of total stress and as a function of long-wave steepness. Error bars indicating 90 % confidence as shown where these could be computed. Black diamonds, Bole 1967; black open squares, Wilson *et al.* 1972; black open circles, Banner 1990; black open triangles to left, Bliven *et al.* 1986; upright triangles, Mitsuyasu & Honda, 1982; downward pointing triangles, Mastenbroek *et al.* 1996; solid squares, Banner & Peirson 1998; solid circles, present study. The second-order turbulence closure results computed by Mastenbroek (1996) are shown as open diamonds. The light solid line is equation (11) with $\beta = 32$ and the light dashed line is equation (12) with $\beta_f = 20$ and $\beta_t = 12$. The heavy dot-dash line indicates linear dependence of wave drag on mean steepness, the light dotted line shows the best fit to data with $AK < 0.06$. The triple dotted light lines in the inset panel show the Donelan *et al.* (2006) results (equations (9) and (10)).

3. The streamfunction technique used by Bole (1967) did not record any values of AK less than 0.08 and the drag ratios shown in figure 5 within the window $0.08 < ak < 0.11$ are highly scattered, therefore we will regard 0.11 as the reliable threshold steepness for his data set from this point.

4. Mitsuyasu & Honda's data are consistently greater by a factor of two than other data gathered using the same technique and, at higher steepnesses, yield wave drag substantially in excess of the total stress. Juxtaposing Mitsuyasu & Honda's data in this manner with data gathered under similar conditions confirms the conclusion of Phillips (1985, p. 510) that the growth rates implied by this data set are too high – indeed, the growth rates appear to be exactly double those indicated by the other data sets. In spite of careful re-examination of the entire data set, we were unable to develop a defensible corrective scheme for their observations and will not use them further to develop quantitative conclusions.

5. The Plant normalization captures the overall trends in the data well across a steepness range $0.05 < AK < 0.12$, but degrades at very low and very high mean steepnesses.

6. The consistency of the remaining data sets is extremely encouraging. Of special note is the computed development of wave drag at very low steepnesses shown in the inset panel. Very different wind and wave conditions prevailed during the Wilson *et al.*

(1973, very short waves, smooth surfaces) and this present study (longer waves, surface populated by microscale breaking waves). For reference, the wave drag predicted by a linear dependence on mean steepness (heavy dash-dot line) is also shown. The best-fit line to the data with $AK < 0.06$ is shown as a dotted line and the best fit is obtained with an exponent of 1.8.

7. The Donelan *et al.* (2006) data can only be compared approximately with the results of this study. Their field data were obtained with steepness levels of the peak waves in the range 0.015 to 0.060 (their figure 3) and wind forcing and peak spectral frequency levels that can be obtained from their table 1. Assuming $U_{\lambda/2} \approx 0.7U_{10}$ yields values $(U_{\lambda/2} - c)/u_*^a$ very close to 12.1. Their growth formula (equation (9)) can be transformed to:

$$\frac{\tau_{wave}}{\tau} = \frac{G(AK)^3}{2}\left(\frac{U_{\lambda/2} - c}{u_*^a}\right)^2, \tag{14}$$

with G taking the values shown in (10). As shown in the inset panel in figure 5, this is very benign normalized forcing in comparison with the data assembled during this study.

Belcher (1999) developed a theoretical framework that incorporated a wave coherent tangential stress contribution as well as a modification to the turbulent stress adjacent to the interface. This yielded an expression equivalent to:

$$\frac{S_{in}(\omega)}{c(\omega)\tau} = \frac{\tau_{wave}}{\tau} = \frac{(\beta_f + \beta_t)(AK)^2}{2 + \beta_f(AK)^2}, \tag{15}$$

where the subscripts f and t denote the contributions to the normalized growth rate of form drag and tangential stress, respectively. Unfortunately, he was unable to obtain direct estimates of these factors analytically. Using (15) and attributing 37.5 % of the Plant growth rate to the wave coherent tangential stress (to best represent the overall data trend at higher steepnesses) yields the light dashed line shown in figure 5. At very low steepnesses, the differences between (13) and (15) are negligible and therefore this curve is not visible in the inset panel.

Shown also in figure 5 is the numerically predicted behaviour of Mastenbroek (1996) for $c/u_a^* = 5$. In this normalization, it is apparent that the primary source of disparity between theory and measurement occurs for AK less than 0.25.

With these promising developments, we return to examine the normalized growth rates as a function of steepness (figure 6). For the reasons stated above, the Mitsuyasu & Honda and lower-steepness Bole data have been eliminated from the ensemble. From this emerges an orderly picture of slow wave growth.

1. The data gathered during this present study collapse reasonably across the entire range of measured mean steepness. A common curve could be fitted which would be encompassed by the computed error bars.

2. Below $AK = 0.10$, normalized growth rates are approximately equal to or greater than the Plant mean value indicated as a light solid line in figure 6.

3. Equation (15) with 37.5 % of normalized growth attributed to wave-coherent tangential stress (shown as a dashed line) provides a reasonable representation of the data at high steepnesses but poor representation of the data at low steepnesses. As the Belcher (1999) analysis is weakly nonlinear, this agreement is encouraging, but not anticipated.

4. For $AK > 0.10$, normalized growth rates are approximately equal to or less than the Plant mean value except for the data of Mastenbroek *et al.* (1996). Potentially, a smooth curve could be drawn which follows the dashed line at higher steepnesses,

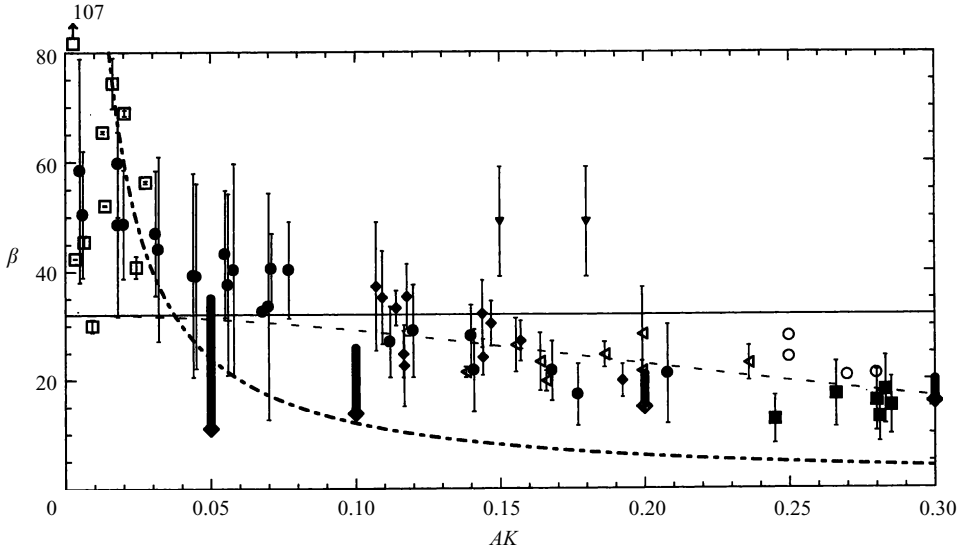

FIGURE 6. Normalized growth plotted as a function of long-wave steepness. Annotations are as in figure 5. The solid vertical bars indicate the total growth obtained if the numerical values of Mastenbroek (1996) are supplemented by a wave-coherent tangential stress obtained from (22).

but rises to a value of approximately $\beta = 55$ at very low slope. Such a curve would be close to being encompassed by the error bars of almost all the data except that of Wilson *et al.* (1973) and Mastenbroek *et al.* (1996).

5. Mastenbroek *et al.* (1996) and Banner (1990) were the only data sets obtained from near-surface pressure measurements. There are two plausible interpretations of the inconsistency between the Mastenbroek *et al.* (1996) measurements and the other data: either their extrapolations to the surface have over-estimated the surface pressure, or, turbulent dissipation of the wave field is a relatively strong process (Teixeira & Belcher 2002; Peirson *et al.* 2003). Stronger turbulent dissipation would be anticipated for the Banner (1990) conditions, yet his data are in good agreement with the rest of the data set. More detailed examination of the static pressure measurements at lower mean steepness levels, accompanied by a critical re-examination of the growth measurements of Mastenbroek *et al.* (1996), will be required to resolve this question.

5.2. *Sheltering*

These data could potentially be interpreted in terms of the Jeffreys (1925) and Belcher & Hunt (1993) concepts of separated and non-separated sheltering. Wind speeds at appropriate reference levels must be computed. Unfortunately, neither roughness lengths in the air nor velocity profiles are presented in Bliven *et al.* (1986) and no further analysis with this data set can be accomplished.

Wave-induced pressure fluctuations are negligible at a distance approximately half a wavelength ($\lambda/2$) above the mean water level (e.g. Mastenbroek *et al.* 1996, figure 8 indicates $\sim\lambda/\pi$) and this has been selected as an appropriate reference level by some investigators. In figure 7, sheltering coefficients (equation (8)) are determined from the available data. In spite of the systematic collapse that is obtained from the present data set, this is not a promising normalization when reconciled against the limited other available data. The Banner (1990) data suggest a significant increase in sheltering

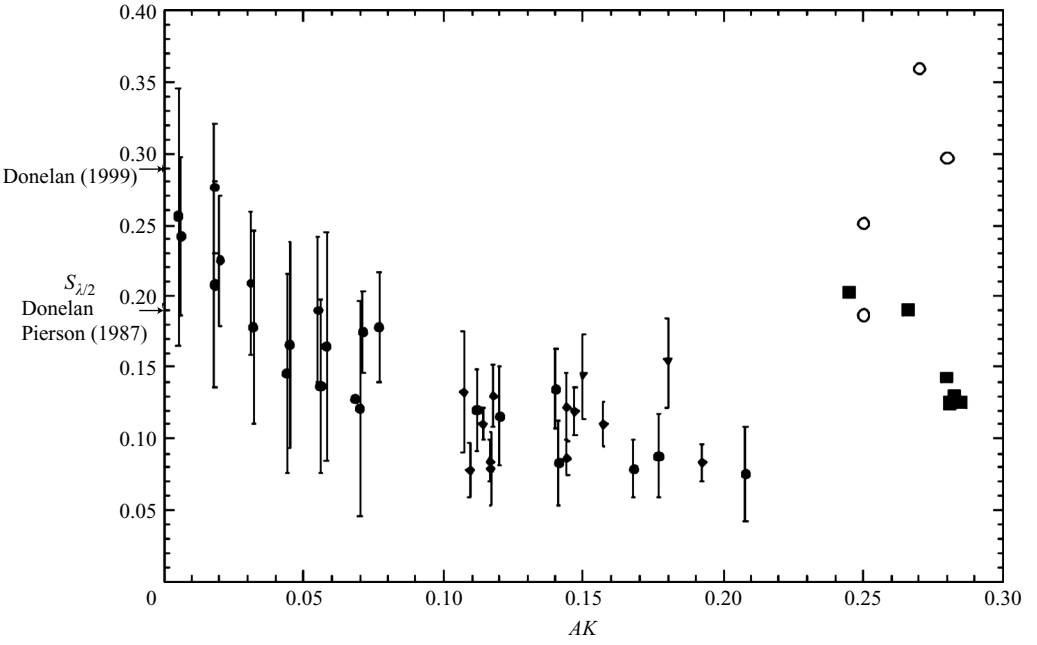

FIGURE 7. Sheltering coefficient at half-wavelength elevation plotted as a function of long-wave steepness. Annotations are as in figure 5. The growth coefficients obtained by Donelan & Pierson (1987) and Donelan (1999) are indicated.

coefficient with the onset of microscale breaking (at approximately, $AK = 0.26$) which may explain the significant differences in sheltering coefficient indicated by the other data sets and the value determined by Donelan (1999). Donelan & Pierson (1987) obtained their value from electromagnetic microwave-scattering techniques and it is in good agreement with the equivalent sheltering coefficient computed from low mean steepness data obtained during this present study.

Figure 8 shows the sheltering coefficients computed from the data when referenced against U_{10}, the customary field reference height. This normalization appears more promising. A constant sheltering coefficient $s_{10} = 0.050$ comes close to being encompassed by the error bars of all available data above a mean steepness of 0.10. Of significance is that a single sheltering coefficient is able to characterize the Banner (1990) data for the both the unbroken (non-separated airflow) and actively breaking (separated airflow) states.

Jeffreys (1925) originally posited his growth formulation on the assumption of fully separated air flow and, by implication, negligible tangential stress. The apparent clustering of the sheltering coefficient in figure 8 includes the Banner & Peirson (1998) data which explicitly has a wave-coherent tangential component with the long-wave data of Bole and this present study wherein the conditions of wave breaking (and therefore air flow separation, Banner 1990) were explicitly avoided. These data provide indirect support for Belcher & Hunt's conclusion that non-separated sheltering is important.

In view of the findings of van Gastel *et al.* (1985) and Meirink & Makin (2002), that the wave Reynolds number is the appropriate normalization for considering wave growth rates of very short waves, we compare their results with relevant collated data in figure 9. The measurements of Banner (1990) and Banner & Peirson (1998) appear

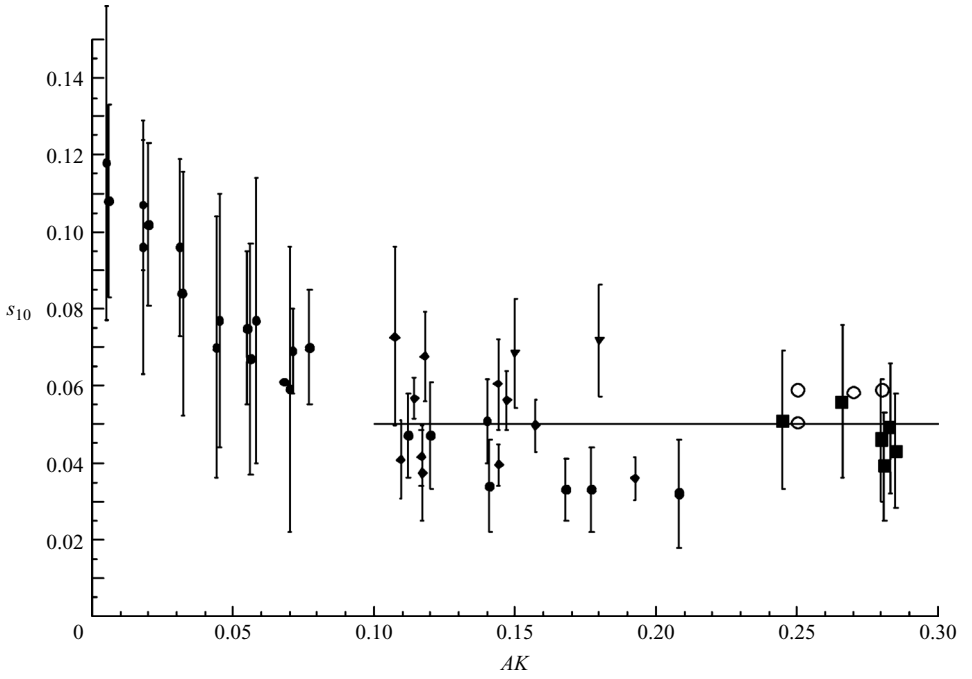

FIGURE 8. Sheltering coefficient at 10 m elevation plotted as a function of long-wave steepness. Annotations are as in figure 5. The heavy line is a best fit to the data of steepness greater than 0.10 and has a value of 0.05.

to be in accord with the modelling studies although it is not immediately apparent why each data set seems to be better represented by the low- or high-Reynolds-number models, respectively.

Of greater significance is the gap between the theoretical/numerical growth rates and the measurements of Wilson *et al.* (1973). The measurements show systematic wave drag development as a function of AK (figure 5) whereas Meirink & Makin (2002, p. 158) found that their computed normalized growth rates were independent of AK ($AK < 0.1$). This implies that the model results would produce a family of quadratic curves in figure 5, each curve determined by its wave Reynolds number. Van Gastel *et al.* (1985) found agreement within 20 % with Miles (1962) but Wilson *et al.* (1973) concluded that Miles (1962) significantly over-estimated their observed growth rates. The findings of these studies must be carefully re-examined, but this is beyond the scope of this investigation.

6. Discussion

6.1. *Wave-coherent tangential stress*

The measurements of Wilson *et al.* (1973) and this present study both indicate very similar normalized wave drag development at very low wave steepnesses (figure 5). With the present understanding of wave growth, this should not be regarded as having more than parametric value. The surface conditions of these two experiments are very different: the Wilson *et al.* waves would have had very close to smooth surfaces whereas the long waves in the present study emerged from a field of steep actively breaking microscale wind waves.

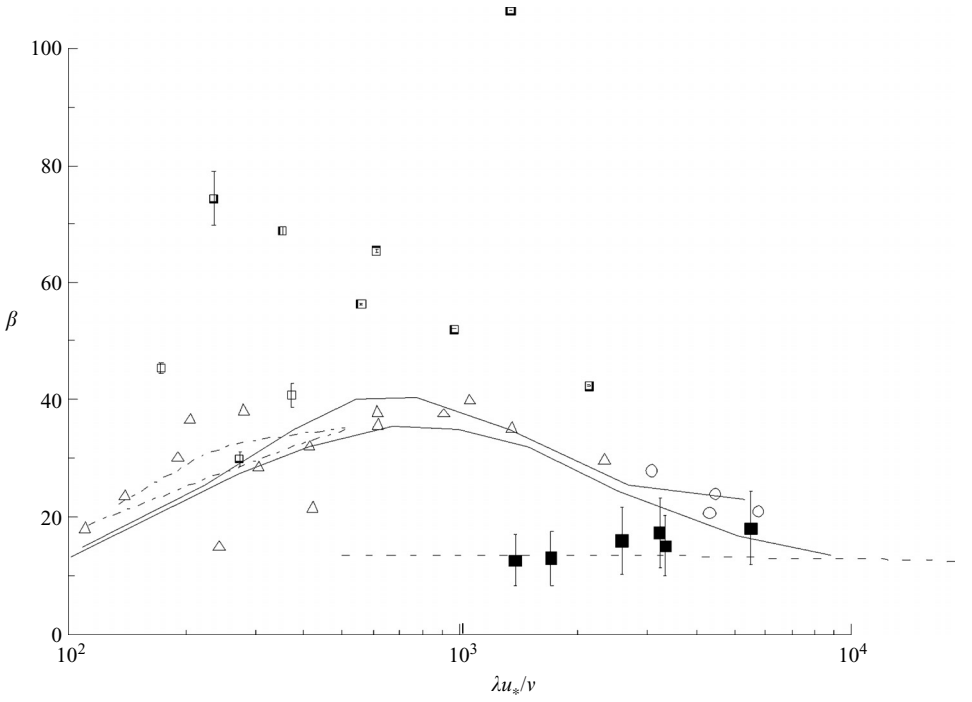

FIGURE 9. Comparison of normalized growth rates computed from the data assembled during this investigation with the findings Meirink & Makin (2000). Their low-Reynolds-number-model results are shown as a solid line and their high-Reynolds-number-model values are shown as a dashed line. The theoretical results of van Gastel *et al.* (1985) are shown as dash-dotted line. The data assembled by Meirink & Makin (2000) are shown as open triangles. Data assembled during this investigation are as follows: black open squares, Wilson *et al.* 1973; black open circles, Banner 1990; solid squares, Banner & Peirson 1998.

If the surface of the waves is smooth, only modulation of the tangential stress by the wave forms can create a wave-coherent tangential stress. The only direct measurements are those of Banner & Peirson (1998) which show that the phase-averaged maximum tangential stress is approximately twice the mean tangential stress (their figure 5). Assuming the notional model of Garrett & Smith (1976) as an approximation to the Banner & Peirson data:

$$\tau_{tang} = \langle \tau_{tang} \rangle (1 + b \cos\theta) \tag{16}$$

would yield:

$$\frac{\tau_{tang,wc}}{\tau} = 0.5AK; \quad b = 1, \tag{17}$$

which would significantly over-estimate the measured growth rates of Wilson *et al.* at their lowest steepness values (inset figure 5). Alternatively, the microscale breaking waves of Banner & Peirson had mean steepnesses in the vicinity of 0.25. Assuming that b increases linearly with mean steepness yields:

$$\frac{\tau_{tang,wc}}{\tau} = 2(AK)^2; \quad b = 4AK, \tag{18}$$

which would significantly underestimate the measured values by an order of magnitude (inset figure 5).

This issue will not be resolved without direct measurements. Such a study should be straightforward using the techniques of Peirson (1997). The above argument shows that it is not impossible that the wave-coherent tangential stress generates sufficiently high growth rates, but the tangential stress would have to be very strongly modulated by these small waves and in a nonlinear manner.

6.2. *Short-wave breaking coherent with long waves*

A potential mechanism for the strong normalized growth of long waves at low steepnesses is the maser-like behaviour suggested by Longuet-Higgins (1969). We now critically examine these proposals using the data measured during this investigation. Longuet-Higgins (1969, equation (6.2)) predicts a ratio r of the quantity $\omega(ak)^2$ between the crests and troughs of the long waves. Longuet-Higgins's equation (6.2) is dependent on his equation (6.1) and using our capacitance-wave-probe measurements, we have been able to compare predicted values of:

$$\sqrt{r} = \left(\frac{1 + AK}{1 - AK}\right)^2, \tag{19}$$

with the ratio of the measured short-wave energy levels at the crest and trough:

$$\sqrt{r} = \left(\frac{a^2_{crest}}{a^2_{trough}}\right). \tag{20}$$

We undertook this as follows.

1. The mean water-surface elevation was computed and deducted from each wave record.
2. The spectral peak energy associated with the fundamental mode of the long waves was extracted from conventional wave spectra. Only the immediately adjacent spectral frequency bins were included with the peak, to account for potential leakage.
3. The inverse transforms of both the extracted long-wave contribution and the remainder of the spectrum were computed.
4. The sequential -90° phase points were identified by consecutive zero downcrossings in the extracted long-wave time series.
5. Using 60° phase bins, the instantaneous energy density of each point in the short-wave time series was binned according to its corresponding phase in the long-wave record.
6. The mean energy density within each phase bin was calculated as the mean square water-surface elevation relative to the long-wave water-surface record.
7. The quantity $\sqrt{r}$ was computed as the ratio of the energy in the crest and trough bins for each wave record.

The measured values of $\sqrt{r}$ and those predicted from the corresponding measurement of long-wave steepness (equation (19)) are shown in figure 10. Values above $AK = 0.10$ should be treated with caution as the fundamental sidebands and the long-wave harmonics have the potential to contaminate this measurement (figure 2*b*). Figure 10 shows that the model assumed by Longuet-Higgins (1969) is encompassed by the error bars of almost all the short-wave data up to a long-wave steepness of approximately 0.17.

We endeavoured to test the different predictions of an asymmetry in the short-wave energy about the long-wave crests provided by Longuet-Higgins and Garrett & Smith. Apart from observing that the distributions of short-wave energy were approximately sinusoidal (Garrett & Smith 1976, p. 929), further examination of the data did not prove fruitful. Much longer data ensembles will be required to resolve

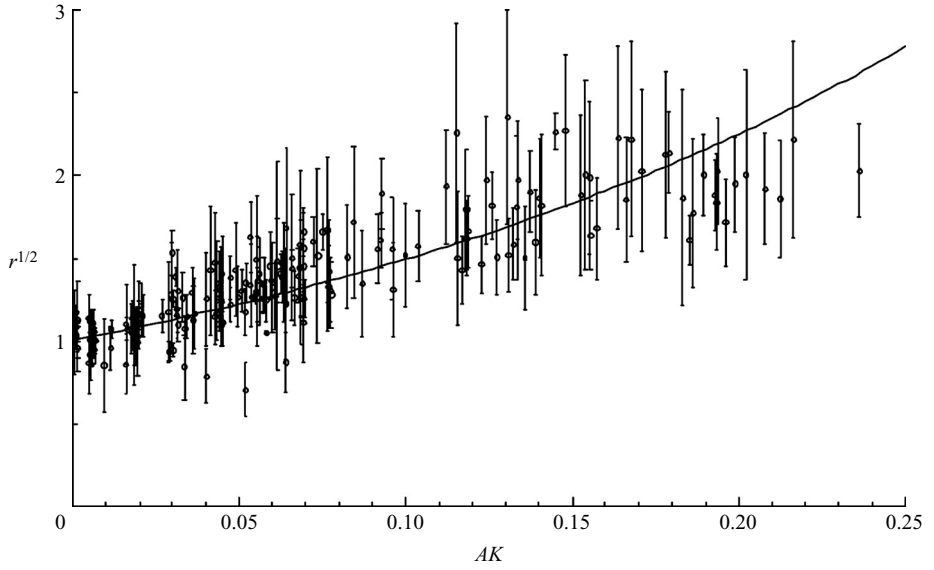

FIGURE 10. Comparison of the ratio of short-wave energy at the crest and troughs of long waves measured during this investigation (open circles) and the predictions of Longuet-Higgins (1969).

the precise distribution of short-wave energy along monochromatic long waves. A complementary investigation by Miller *et al.* (1991) found that the modulation of short-wave energy by low-frequency (0.5 Hz) long waves was in agreement with the predictions of Longuet-Higgins & Stewart (1960) provided that the wind forcing was not too strong.

Having extracted the short-wave energy from the long waves, it was a relatively straightforward process to examine the predictions of Phillips & Banner (1974), as shown in figure 11. Very poor correlations were obtained at the first wave probe, possibly because there was insufficient fetch to develop microscale breaking waves in the absence of long waves. For $AK > 0.10$, the predictions deteriorated owing to spectral leakages associated with side band development and nonlinearity. An unknown parameter in the Phillips/Banner model is the ratio b of the magnitude of the wind drift to the friction velocity in the air. Phillips & Banner (1974) quote $b = 0.55$ based on punch card measurements, Wright (1976) quotes values declining from $b = 0.73$ to 0.50 with increasing wind speed based on thin paraffin disks, and Peirson & Banner (2003) found $b = 0.30 \pm 0.10$ from extrapolations of particle image velocimetry (PIV) measurements within the aqueous viscous sublayer to the instantaneous surface along wind-forced microscale breaking waves. No direct measurements were undertaken during this study. The predictions shown in figure 11 were obtained assuming a constant value of $b = 0.58$.

The Longuet-Higgins model of short-wave modulation and the Phillips/Banner model of short-wave energy reduction due to the presence of the long waves provide good representations of the measured data. Why then, did Wright (1976) find such poor agreement with the Phillips/Banner model? The answer to this can be found by considering the wind-induced growth rate as suggested by Wright in his closing remarks and the conclusions of Miller *et al.* (1991). We have extended Miller *et al.*'s

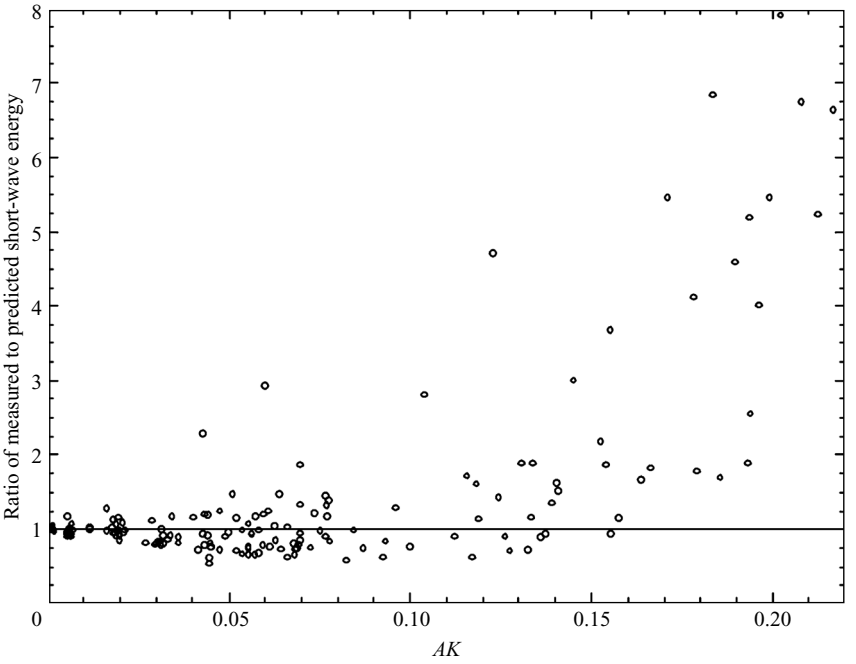

FIGURE 11. Ratio of short-wave energy measured during this investigation compared with the predictions of Phillips & Banner (1974) using a single value of $b = 0.058$. Data from the wave probe of shortest fetch have not been included. Two other data points from the entire data set are not encompassed within the graph limits.

work by quantitatively summarizing the important time scales in figure 12, and use it to interpret the findings of other investigators.

There are at least two critical time scales that characterize interactions between long and short waves in the presence of wind.

1. The period of the long waves ($T = 1/F$), which is approximately the time taken for a full long-wave cycle to pass beneath a short-wave (assuming sufficient separation of wave scales).

2. A characteristic growth time scale for the wind waves due to the action of the wind.

If wind-wave growth can be normalized in the form of (7), we can define a time scale for a wind wave to increase in energy by a factor e:

$$t_e = \frac{\rho_w g^2}{8\pi^3 \beta \tau f^3}. \tag{21}$$

In figure 12, a sequence of diagonal lines show t_e as a function of f for various values of τ selecting $\beta = 20$ as a representative value from figure 6, with other variables taking their conventional values. The selected values of τ correspond approximately to moderate wind forcing and to experimental investigations undertaken in the literature.

Neither air-entraining nor microscale breaking waves occur when the total stress falls below 0.05 Pa (approximately $U_{10} = 5\,\mathrm{m\,s^{-1}}$) and beyond $f = 6\,\mathrm{Hz}$, very strong wind forcing is required to force microscale waves into the microscale breaking state. At the right-hand side of figure 12, these conditions are indicated by the shaded area.

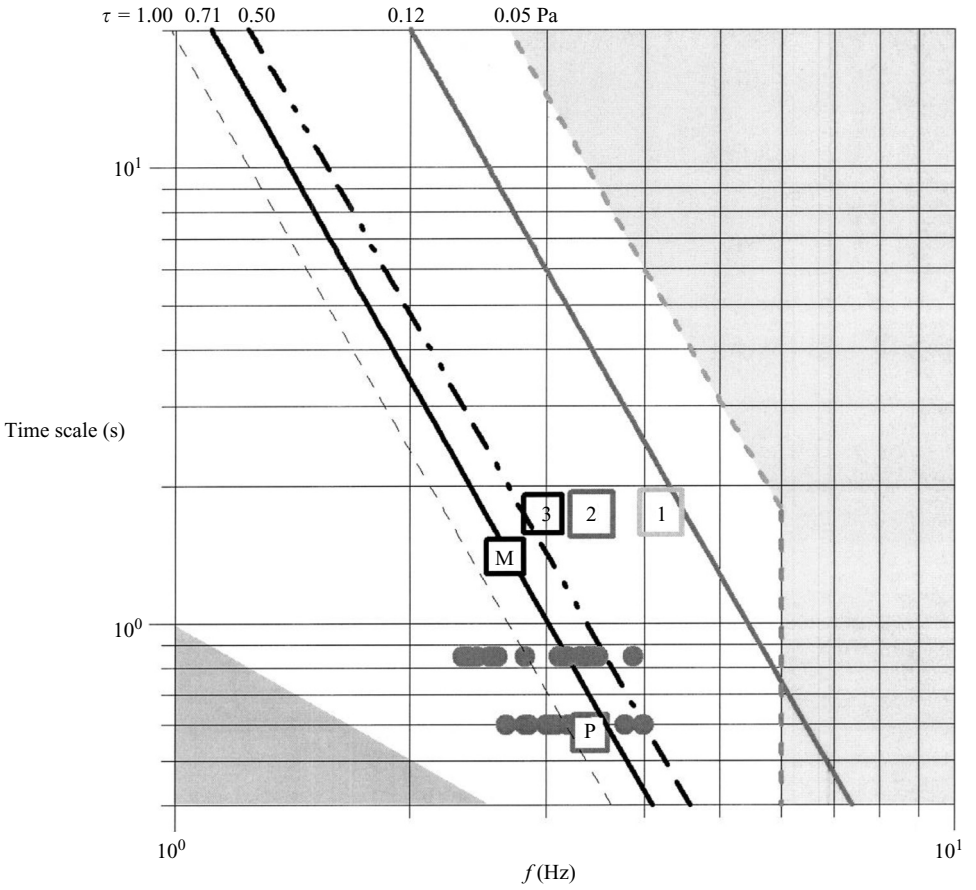

FIGURE 12. Schematic diagram showing interactions between wind-induced growth of short waves and their modulation by long waves. The horizontal axis is the peak frequency of the short waves. The vertical axis shows corresponding time scales. Oblique lines indicate the time scales for short waves to increase their energy by a factor of e at the corresponding wind stress values indicated at the top of the diagram. The shaded region to the right indicates wind stress values and wave frequencies at which small-scale breaking does not occur. The lower left-hand shaded region indicates time scales less than $1/f$. Colours and line styles have been used to indicate correspondence between different levels of wind forcing on this diagram. Light grey '1', Wright 1976, $\tau = 0.033$ Pa. Mid-grey indicates data gathered at approximately $\tau = 0.12$ Pa '2', Wright 1976; 'P', Phillips & Banner 1974; solid circles, present study; Black '3', Wright 1976, $\tau = 0.50$ Pa; Black 'M', Mitsuyasu, 1966, $\tau = 0.71$ Pa, cited in Phillips & Banner 1974.

The shaded lower left-hand side corner of figure 12 indicates the region in which the time scale $= 1/f$.

In figure 12, a number of data sets are shown. The data measured during this study is shown as solid circles and indicates that the period of the long waves is significantly less than the time scale of the short-wave growth. This is consistent with the results shown in figures 10 and 11. The data of Phillips & Banner (1974) were gathered for a similar scale of wave and wind forcing as this study. The long-wave period used by Mitsuyasu (1966) is similar to the estimated short-wave growth time scale as shown in figure 12. Phillips & Banner (1974) found good agreement between his data and their model.

Wright (1976) examined three levels of wind forcing. The lowest (shown as 'W' in light grey in figure 12), was gathered at a modest fetch (1 m, see remarks by Peirson & Banner 2003, p. 7) at a wind stress significantly less than 0.05 Pa. No microscale breaking waves would be anticipated under these conditions. His moderate wind-forcing case showed good agreement with the Phillips & Banner (1974) model, as figure 12 would anticipate. His highest wind case, shows an anticipated short-wave growth time scale less than the period of his long waves. In this case, wind-wave behaviour would be primarily determined by the wind forcing rather than the modulations of the long waves. We concur with his closing remark that the Phillips & Banner theory 'neglects the direct coupling with the wind' and figure 12 is a first step towards determining those regimes in which direct wind forcing or long-wave modulation control the energy levels of shorter waves.

Chen & Belcher (2000) have produced an alternative model of short-wave attenuation in the presence of long waves based on a model of reduced available wave drag to the short waves owing to the presence of the long waves. They do this by considering the wave growth rates of Mitsuyasu & Honda (1982) which have been shown to be implausibly high during this present study. Also, significant short-wave attenuation ($>50\,\%$) occurs prior to the long-wave steepness reaching a value of 0.10, at which point the wave drag absorbed by the long waves is less than 20% of the total stress (figure 4). Consequently, the significant levels of short-wave attenuation observed during this study cannot be explained in terms of the modest reductions observed in the total stress.

6.3. *Long-wave coherent tangential stress contribution*

The Phillips/Banner mechanism provides very efficient triggering of strong fluxes from the short-wave field local to the crest of the long waves where the long-wave coherent effects are greatest. Assuming negligible direct energy flux to the long waves at very low steepnesses and that approximately $40 \pm 10\%$ of the total stress is supported directly via tangential stress that is not coherent with any part of the wave field at this level of wind forcing (Banner & Peirson 1998, figure 11), the ceiling energy input to a field of uniform long waves mediated by wave drag captured by the short-wave field is (Longuet-Higgins 1969, equation (7.6)):

$$S_{in} = (0.6 \pm 0.1)\tau AKC, \tag{22}$$

or,

$$\frac{\tau_{wave}}{\tau} = (0.6 \pm 0.1)AK, \tag{23}$$

or,

$$\beta = \frac{(1.2 \pm 0.2)}{AK}. \tag{24}$$

The mean value curves have been added to figures 5 and 6 as heavy dash-dotted lines. At very low steepnesses ($AK \sim 0.005$), the expressions substantially overestimate the wave drag and the normalized growth rate. This may be because the modulations induced by the long waves are weaker than those inherent to the short-wave groups themselves (Banner & Peirson 2007). However, in the range $0.02 < AK < 0.04$, the curves produce a reasonable approximation of the observed wave drag. The singularity in normalized growth at zero steepness makes more detailed comparison at low long-wave steepness more difficult in figure 6. However, it does permit comparison at higher steepness levels.

If the form drag estimates of the numerical modelling are accepted as correct, the data suggest that the form drag of the long waves becomes more significant than the wave-coherent tangential contribution at $AK = 0.07$. Nonetheless, the wave-coherent tangential contribution remains significant at steepnesses greater than 0.10 (the nominated limit to which the present data could be analysed).

Further, note that if the estimates of total normalized growth rate obtained from the numerical modelling of Mastenbroek (1996) have the present estimates of the long wave-coherent tangential contribution added to them, the total is a good approximation of the measured data, as indicated by the vertical bars in figure 5. We note also that the variations in surface roughness implied by modulated short waves with preferential breaking at the crest will further augment the form drag (Mastenbroek 1996, p. 63), placing the diamonds approximately 5 units higher on figure 5.

It should be noted that during this discussion, we have assumed the strongest possible contribution of the short waves to long-wave growth. The cosine variation of the key quantities in relation to the long waves means that shifts in the phase of the short-wave breaking up to approximately 25° will have negligible impact on the results.

To explain their radar observations of wave growth, Plant & Wright (1977, p. 790, 792) hypothesized that short ($\lambda < 0.1$ m) gravity waves grow directly owing to wind input but longer waves received energy flux from shorter, wave components. Their conclusion provides independent support for the quantitative findings of this investigation.

In summary, the observed growth cannot be accounted for by present numerical estimates of wave drag alone. By quantifying the short-wave energy relative to the underlying long waves, short-wave energy levels consistent with Longuet-Higgins (1969) and Phillips & Banner (1974) are found. The measured normalized growth rates are consistent with numerically predicted wave drag (Mastenbroek 1996) supplemented by a significant long-wave-coherent tangential stress as proposed by Longuet-Higgins (1969) and triggered by selective breaking of the short waves at the long-wave crests as proposed by Phillips & Banner (1974).

6.4. *Implications for wave growth in the open ocean*

No measurements of wave growth in the open ocean have been considered during this investigation. Numerical prediction of storm waves requires an integration in both time and space in which the antecedent effects of modest swell steepnesses are important. This study shows that lower-frequency wave growth can be significantly augmented by a systematic response in the shorter scales. Longuet-Higgins (1969) concluded that these mechanisms deserved serious consideration at field scale, but we are not aware of more contemporary comparisons of his ideas with field data sets.

Further, figure 12 has been scaled to indicate the swell time scales of interest along the left-hand axis. The figure indicates that time scales of growth of the higher-frequency components of the spectrum are sufficiently slow to enable modulation and acquisition of shorter-wave energy by the swell to be effective. At very high wind speeds ($\tau > 1.0\,\mathrm{Pa} \sim U_{10} > 20\,\mathrm{m\,s^{-1}}$), the range of higher-frequency waves able to contribute to swell growth significantly reduces with wind speed, suggesting reduced levels of short-wave input to longer waves within intense storms.

Measurement techniques to test these ideas quantitatively has become available. Major studies have been undertaken in which large-scale (Melville & Matusov 2002) breaking has been directly monitored and characterized. Further development of

infrared techniques (Jessup & Phadnis 2005) may enable microscale breaking to be directly quantified under field conditions. To our knowledge, long-wave phase-related measurements of short-wave breaking have not been reported to date, but application of these techniques should make it possible to assess the potential for enhanced growth of longer waves due to short-wave breaking under field conditions.

An ongoing difficulty for work on air–sea interaction has been distinguishing between the defined components contributing to the development of wave spectra under field conditions (equation (3)). This present investigation has resolved some important and long-standing questions regarding the disparity between measured and predicted growth rates of slow waves. In this paper, discussion has been focused around the wind input term (equation (3) right-hand side, term 1). However, the Longuet-Higgins (1969) growth mechanism is a nonlinear spectral interaction (equation (3) right-hand side, term 2) with a cascade of energy from shorter-wave breaking (equation (3) right-hand side, term 3) to lower-frequency waves. Consequently, coupling all three spectral development processes in this manner requires careful re-examination of this particular nonlinear spectral interaction, especially its impact within the high-frequency tail. This process is not explicitly incorporated within present operational wave-prediction models.

7. Conclusions and recommendations

A systematic response of the wind-induced growth of slow waves to their mean steepness can be observed across a range of reported data sets. By carefully examining the normalized wave drag in terms of mean wave steepness, we have been able to clearly identify and eliminate problems with some data sets. However, the input levels measured by Mastenbroek *et al.* (1996) remain to be reconciled with other reliable data.

A systematic decline in normalized growth as a function of steepness can be observed in slow-wave growth data. For mean steepnesses less than 0.3, the normalized growth values span the stated uncertainty in the Plant (1982) data assembly. Very high normalized growth rates have been observed at low mean steepnesses. The collapse of the data as a function of AK yields a potentially-useful parameterization of slow wave normalized wave drag and growth due to wind.

At mean steepnesses greater than 0.13, Jeffreys' sheltering coefficients computed from the data cluster around 0.050 ± 0.005 when using the 10 m elevation wind speed as the reference. This finding lends indirect support for the Belcher & Hunt (1993) concept of non-separated sheltering, but air-sided measurements incorporating separation detection will be required to confirm this result.

Data obtained during this study show quantitative agreement with the predictions of Longuet-Higgins (1969) and Phillips & Banner (1974) of the interactions between short wind waves and longer monochromatic waves. The measured normalized long-wave growth rates are consistent with numerically predicted wave drag (Mastenbroek 1996) augmented by a significant wave-coherent tangential stress as proposed by Longuet-Higgins (1969).

Detailed consideration of the time scales associated with slow long-wave growth shows that there are specific long-wave frequencies that are predicted to exhibit enhanced growth due to wave-coherent short-wave breaking. Beyond the wind input threshold for breaking wave generation, the range of long-wave scales exhibiting enhanced growth due to short-wave breaking reduces with increased wave forcing.

To our knowledge, a key objective of Shemdin & Hsu (1967) and Bole & Hsu (1969) still remains unfulfilled: measurements of form drag in the air have not been reconciled against measurements of net wave growth, except indirectly during this study. Such an investigation remains a high priority for the air–sea interaction community particularly if form drag measurements in the field are to be pursued.

The Longuet-Higgins (1969) mechanism deserves careful re-examination as a significant nonlinear spectral interaction in the open ocean, particularly within the high-frequency tail. With the wave-monitoring techniques presently available, quantitative assessment of these predictions should be possible.

Helpful assistance provided by Professor Hisashi Mitsuyasu and four anonymous reviewers is gratefully acknowledged. W. L. P. would like to thank Professor Michael Banner for encouraging him never to despise the wave-coherent tangential stress and Dr Bruce Cathers for always insisting that he systematically assemble his time and space scales. Technical support for the investigation was provided by Mr Hector Martinez and Mr John Hart and Mrs. Monika Stieler at WRL with funding provided in part by the United States Army through its European Research Office and in part by the Australian Research Council (DP0452505).

REFERENCES

Banner, M. L. 1990 The influence of wave breaking on the surface pressure distribution in wind–wave interactions. *J. Fluid Mech.* **211**, 463–495.

Banner, M. L. & Peirson, W. L. 1998 Tangential stress beneath wind-driven air–water interfaces. *J. Fluid Mech.* **364**, 115–145.

Banner, M. L. & Peirson, W. L. 2007 Wave breaking onset and strength for two-dimensional deep-water wave groups. *J. Fluid Mech.* **585**, 93–115.

Banner, M. L. & Phillips, O. M. 1974 On the incipient breaking of small scale waves. *J. Fluid Mech.* **64**, 647–656.

Belcher, S. E. 1999 Wave growth by non-separated sheltering. *Eur. J. Mech.* B/*Fluids* **18**, 447–462.

Belcher, S. E. & Hunt, J. C. R. 1993 Turbulent shear flow over slow waves. *J. Fluid Mech.* **251**, 109–148.

Belcher, S. E. & Hunt, J. C. R. 1998 Turbulent flow over hills and waves. *Annu. Rev. Fluid. Mech.* **30**, 507–538.

Benjamin, T. B. & Feir, J. E. 1967 The disintegration of wave trains on deep water. Part 1. Theory. *J. Fluid Mech.* **27**, 417–430.

Bliven, L. F., Hwang, N. E. & Long, S. R. 1986 Experimental study of the influence of wind on Benjamin–Feir sideband instability. *J. Fluid Mech.* **162**, 237–260.

Bole, J. B. 1967 Response of gravity water waves to wind excitation. PhD thesis, Dept of Civil Engineering, Stanford University.

Bole, J. B. & Hsu, E. Y. 1969 Response of gravity water waves to wind excitation. *J. Fluid Mech.* **35**, 657–675.

Chen, G. & Belcher, S. E. 2000 Effects of long waves on wind-generated waves. *J. Phys. Oceanogr.* **30**, 2246–2256.

Donelan, M. A. 1990 Air–sea interaction. In *The Sea: Ocean Engineering Science*, vol. 9, pp. 239–292. Wiley.

Donelan, M. A. 1999 Wind-induced growth and attenuation of laboratory waves. In *Wind-over-Wave Couplings: Perspectives and Prospects* (ed. Sajjadi *et al.*), pp. 183–194. Clarendon.

Donelan, M. A. & Pierson, W. J. 1987 Radar Scattering and equilibrium ranges in wind-generated waves with application to scatterometry. *J. Geophys. Res.* **92**, C5, 4971–5029.

Donelan, M. A., Babanin, A. V., Young, I. R. & Banner, M. L. 2006 Wave-follower field measurements of the wind-input spectral function. Part II: Parameterisation of wind input. *J. Phys. Oceanogr.* **36**, 1672–1689.

van Duin, C. 1996 Rapid-distortion turbulence models in the theory of surface-wave generation. *J. Fluid Mech.* **329**, 147–153.

Duncan, J. H. 1983 The breaking and non-breaking resistance of a two-dimensional hydrofoil. *J. Fluid Mech.* **126**, 507–520.

Garrett, C. & Smith, J. 1976 On the interaction between long and short surface waves. *J. Phys. Oceanogr.* **6**, 925–930.

van Gastel, K., Janssen, P. A. E. M. & Komen, G. J. 1985 On phase velocity and growth rate of wind-induced gravity-capillary waves. *J. Fluid Mech.* **161**, 199–216.

Hasselmann, D. & Bösenberg, J. 1991 Field measurements of wave-induced pressure over wind-sea and swell. *J. Fluid Mech.* **230**, 391–428.

Hasselmann, K. 1971 On the mass and momentum transfer between short gravity waves and larger-scale motions. *J. Fluid Mech.* **50**, 189–205.

Holthuijsen, L. H. & Herbers, T. H. C. 1986 Statistics of wave breaking observed as whitecaps on the open sea. *J. Phys. Oceanogr.* **16**, 290–297.

Jähne, B. & Haußecker, H. 1998 Air-water gas exchange. *Annu. Rev. Fluid Mech.* **30**, 444–468.

Janssen, P. 2004 *The Interaction of Ocean Waves and Wind*. Cambridge University Press.

Jeffreys, H. 1925 On the formation of water waves by wind. *Proc. R. Soc. Lond.* **107**, 189–206.

Jessup, A. T. & Phadnis, K. R. 2005 Measurement of the geometric and kinematic properties of microscale breaking waves from infrared imagery using a PIV algorithm. *Meas. Sci. Techol.* **16**, 1961–1969.

Katsaros, K. B. & Atatürk, S. S. 1992 Dependence of wave-breaking statistics on wind stress and wave development. In *Breaking Waves* (ed. M. L. Banner & R. H. J. Grimshaw). Springer.

Kinsman, B. 1984 *Wind Waves*. Dover.

Komen, G. J., Cavaleri, M., Donelan, M., Hasselmann, K., Hasselmann, S. & Janssen, P. A. E. M. 1994 *Dynamics and Modelling of Ocean Waves*. Cambridge University Press.

Larson, T. R. & Wright, J. W. 1975 Wind-generated gravity–capillary waves: laboratory measurements of temporal growth rates using microwave backscatter. *J. Fluid* Mech. **70**, 417–436.

Li, P. Y., Xu, D., & Taylor, P. A. 2000, Numerical modelling of turbulent airflow over water waves. *Boundary-Layer Met*. **95**, 397–425.

Longuet-Higgins, M. S. 1960 Mass-transport in the boundary-layer at a free oscillating surface. *J . Fluid Mech.* **8**, 293–306.

Longuet-Higgins, M. S. 1969 A non-linear mechanism for the generation of sea waves. *Proc. R. Soc. Lond.* A **311**, 371–389.

Longuet-Higgins, M. S. 1992 Capillary rollers and bores. *J. Fluid Mech.* **240**, 659–679.

Longuet-Higgins, M. S. 1995 Parasitic capillary waves: a direct calculation. *J. Fluid Mech.* **301**, 79–107.

Longuet-Higgins, M. S. & Stewart, R. W. 1960 Changes in the form of short gravity waves on long waves and tidal currents. *J. Fluid Mech.* **8**, 565–583.

Makin, V. K. & Kudryavtsev, V. N. 2002 Impact of dominant waves on sea drag. *Boundary-Layer Met*. **103**, 83–99.

Makin, V. K., Branger, H., Peirson, W. L. & Giovanangeli, J. P. 2007 Modelling of laboratory measurements of stress in the air flow over wind-generated and paddle waves. *J. Phys. Oceanog*. **37**, 2824–2837.

Mastenbroek, C. 1996 Wind wave interaction. PhD thesis, Delft Technical University.

Mastenbroek, C., Makin, V. K., Garat, M. H. & Giovanangeli, J. P. 1996 Experimental evidence of the rapid distortion of turbulence in the air flow over water waves. *J. Fluid Mech.* **318**, 273–302.

Meirink, J. F. & Makin, V. K. 2000 Modelling low-Reynolds-number effects in the turbulent air flow over water waves. *J. Fluid Mech.* **415**, 155–174.

Melville, W. K. & Matusov, P. 2002 Distribution of breaking waves at the ocean surface. *Nature* **417**, 58.

Miles, J. W. 1957 On the generation of surface waves by shear flows. *J. Fluid Mech.* **3**, 185–204.

Miles, J. W. 1962 On the generation of surface waves by shear flows. Part 4. *J. Fluid Mech.* **13**, 443–448.

Miles, J. W. 1993 Surface-wave generation revisited. *J. Fluid Mech.* **256**, 427–441.

Miles, J. W. 1996 Surface-wave generation: a viscoelastic model. *J. Fluid Mech.* **322**, 131–145.

Miller, S. J., Shemdin, O. H., Longuet-Higgins, M. S. 1991 Laboratory measurements of modulation of short wave slopes by long surface waves. *J. Fluid. Mech.* **233**, 389–404.

Mitsuyasu, H. 1966 Interactions between water waves and wind (I). *Rep. Res. Inst. Appl. Mech., Kyushu University*, **14**, 67–88.

Mitsuyasu, H. & Honda, T. 1982 Wind-induced growth of water waves. *J. Fluid Mech.* **123**, 425–442.

Okuda, K., Kawai, S. & Toba, Y. 1977 Measurement of skin friction distribution along the surface of wind waves. *J. Oceanogr. Soc. Japan* **30**, 190–198.

Peirson, W. L. 1997 Measurement of surface velocities and shears at a wavy air–water interface using particle image velocimetry. *Exps. Fluids* **23**, 427–437.

Peirson, W. L. & Banner, M. L. 2003 Aqueous surface layer flows induced by microscale breaking wind waves. *J. Fluid Mech.* **479**, 1–38.

Peirson, W. L. & Belcher, S. E. 2005 Growth response of waves to the wind stress. *Proc. Intl Conf. Coastal Engng*. ASCE.

Peirson, W. L., Garcia, A. W. & Pells, S. E. 2003 Water–wave attenuation due to opposing wind. *J. Fluid Mech.* **487**, 345–365.

Peirson, W. L., Branger, H., Giovanangeli, J. P. & Banner, M. L. 2004 The response of wind drag to underlying swell slope. WRL Res. Rep. 223, University of New South Wales, Water Research Laboratory, Manly Vale NSW, Australia. ISBN 0 85 824 030 2.

Phillips, O. M. 1963 On the attenuation of long gravity waves by short breaking waves. *J. Fluid Mech.* **16**, 321–332.

Phillips, O. M. 1977 *The Dynamics of the Upper Ocean*. Cambridge University Press.

Phillips, O. M. 1985 Spectral and statistical properties of the equilibrium range in the wind-generated gravity waves. *J. Fluid Mech.* **156**, 505–531.

Phillips, O. M. & Banner, M. L. 1974 Wave breaking in the presence of wind drift and swell. *J. Fluid Mech.* **66**, 625–640.

Plant, W. J. 1982 A relationship between wind stress and wave slope. *J. Geophys. Res.* **87**, C3, 1961–1967.

Plant, W. J. & Wright, J. W. 1977 Growth and equilibrium of short gravity waves in a wind-wave tank. *J. Fluid Mech.* **82**, 767–793.

Rapp, R. J. & Melville, W. K. 1990 Laboratory measurements of deep water breaking waves. *Phil. Trans. R. Soc. Lond.* A **331**, 735–800.

Robinson, I. & Guymer, T. 1996 Observing oceans from space. In *Oceanography: An Illustrated Text*. (ed. C. P. Summerhayes & S. A. Thorpe) Chap. 3. John Wiley.

Reul, N., Branger, H. & Giovanangeli, J-P. 2007 Air flow structure over short-gravity breaking water waves. *Boundary-Layer Met.* doi 10.1007/s10546-007-9240-3.

Shemdin, O. H. & Hsu, E. Y. 1967 Direct Measurements of aerodynamic pressure above a simple progressive gravity wave. *J. Fluid Mech.* **30**, 403–416.

Shyu, J.-H. & Phillips, O. M. 1990 The blockage of gravity and capillary waves by longer waves and currents. *J. Fluid Mech.* **217**, 115–141.

Snyder, R. L., Dobson, F. W., Elliott, J. A. & Long, R. B. 1981 Array measurements of atmospheric pressure fluctuations above surface gravity waves. *J. Fluid Mech.* **102**, 1–59.

Teixeira, M. A. & Belcher, S. E. 2002 On the distortion of turbulence by a progressive surface wave. *J. Fluid Mech.* **458**, 229–267.

Townsend, A. A. 1972 Flow in a deep turbulent boundary layer over a surface distorted by water waves. *J. Fluid Mech.* **55**, 719–735.

Van Dorn, W. G. 1966 Boundary dissipation of oscillatory waves. *J. Fluid Mech.* **24**, 769–779.

Wilson, W. S., Banner, M. L., Flower, R. J., Michael, J. A. & Wilson, D. G. 1973 Wind-induced growth of mechanically generated water waves. *J. Fluid Mech.* **58**, 435–460.

Wright, J. W. 1976 The wind drift and wave breaking. *J. Phys. Oceanog.* **6**, 402–405.

Wu, H.-Y., Hsu, E.-Y. & Street, R. L. 1979 Experimental study of non-linear wave-wave interaction and white-cap dissipation of wind-generated waves. *Dyn. Atmos. Oceans* **3**, 55–78.

Wu, H.-Y., Hsu, E.-Y. & Street, R. L. 1977 The energy transfer due to air-input, non-linear wave-wave interactions and white-cap dissipation associated with wind-generated waves. *Dept Civ. Engng Tech. Rep.* 207, Stanford University, CA.